High-Temperature Nano-Derived Micro-H_2 and -H_2S Sensors

Engin Ciftyurek (Graduated Student, Ph.D.)
Christina Wildfire (Graduated Student, Ph.D.)
Edward M. Sabolsky (PI)

Energy Materials Program
Department of Mechanical and Aerospace Engineering
West Virginia University

Annual DOE-NETL University Coal Research Project Review
May 19-21, 2014

Objectives

- Develop micro-scale, chemical sensors composed of nano-derived, metal-oxide materials which display stable performance within high-temperature environments (>500°C).
- Short term– Develop high-temperature H_2, SO_2, and H_2S sensor using low cost, easily reproducible methods with 3D porous nanomaterials.
- Long term – Develop high-temperature micro-sensor arrays to detect gases such as NO_x, SO_x, H_2S, H_2, HCs.
- Collaboration with NexTech Materials, Ltd. (Lewis Center, OH).

Proposed Work Plan

Task 2.0 Synthesis and Characterization of Nano-Composite Electrodes. Doped-tin oxide, ceria, zirconate, and molybdate/tungstate nanomaterials will be synthesized using hydrothermal and/or glycine-nitrate processes and characterized.

Task 3.0 Lost-Mold Microcasting of the Selective Electrode Structure. Develop microcasting methods for patterning microscale, chemically selective pads on alumina wafers.

Task 4.0 Fabrication of Micro-Sensors and Arrays. Fabricate functional hydrogen micro-sensors and micro-sensor arrays. In addition, stable IDEs for high-temperature applications must be developed.

Task 5.0 Micro-Sensor and Sensor Array Testing.
Micro-sensors will be first characterized for baseline resistance using external furnace heat at temperatures ranging from 600°C to 1000°C.

Proposed Milestones

- Sensor and Sensor Array design established – **Q2**
- Process for synthesizing nanomaterials established – **Q4**
- Stability of nanomaterials electrodes defined– **Q8**
- Micro-casting process defined – **Q6**
- Micro-sensors fabricated – **Q8**
- Micro-sensor array fabricated – **Q9**
- Micro-sensor specification targets achieved – **Q11**

Proposed Deliverables

1) Quarterly and annual progress reports to DOE

2) Subtask 2.2- industrial partner delivers nanomaterials to WVU for stability testing ***(Q3)***

3) Subtask 3.1- Micro-molds delivered to industrial partner for commercial microcasting demonstration ***(Q5-8)***

4) Subtask 5.1- Delivery of micro-sensors to industrial partner for testing ***(delivery start of each quarter Q7-Q11)- plan on sending more arrays to collaborator over the summer.***

Presentations of this Work

1. "High temperature nano-derived hydrogen sensors," Christina Wildfire, Engin Ciftyurek, Katarzyna Sabolsky, Edward M. Sabolsky, European Ceramics Society (ECerS) XII conference in Stockholm, Sweden, June 19-23 2011, Nanomaterials Symposium; **INVITED PRESENTATION**

2. "Performance and Stability of High-Temperature Nano-Derived Hydrogen Sensors," Edward M. Sabolsky, Christina Wildfire, Engin Ciftyurek, Katarzyna Sabolsky, 220th Electrochemical Society Meeting, Boston, MA, Oct. 9-14, 2012; **PRESENTATION**

3. "High-Temperature Nanomaterials for Electrochemical Micro-Sensors," Edward M. Sabolsky, Christina Wildfire, Engin Ciftyurek, Energy Materials and Applications (EMA) 2012 Conference in Orlando, FL, January 18-20, 2012, S1: New Frontiers in Electronic Ceramic Structures, Advanced Electronic Material Devices and Circuit Integration; **PRESENTATION**

4. "Nano-Derived, Micro-Chemical Sensors for High-Temperature Applications," Edward M. Sabolsky, Christina Wildfire, Engin Ciftyurek, Katarzyna Sabolsky, 221st Electrochemical Society Meeting in Seattle, WA, May 6-10, 2012; **INVITED PRESENTATION**

5. "High-Temperature Nano-Derived Chemical Micro-Sensors," Edward M. Sabolsky, Christina Wildfire, Engin Ciftyurek, Katarzyna Sabolsky, 10th International Symposium on Ceramic Materials and Components for Energy and Environmental Applications (CMCEE) 2012 in Dresden, Germany, May 20-23, 2012; **PRESENTATION**

Presentations of this Work

6) "High-Temperature Compatible Electrodes with Various Microstructural Architectures," E. Çiftyürek, K. Sabolsky, and E.M. Sabolsky, 221st Electrochemical Society Meeting in Seattle, WA, May 6-10, 2012; **PRESENTATION**.

7) "Degradation of Platinum Thin Films Electrodes for High-Temperature MEMS Applications", E. Çiftyürek, K. Sabolsky and E. M. Sabolsky, WV Academia Science 2012 Charleston, West Virginia, USA. **PRESENTATION**.

8) "High-Temperature Nano-Derived Sensors for Online Monitoring of SO_2 Emissions", E. Çiftyürek, C. Wildfire, and E. M. Sabolsky, Materials Science & Technology 2012, Pittsburgh, Pennsylvania, USA. **PRESENTATION**.

9) "High-Temperature Nano-derived Sensor Development for Detection of H_2S and SO_2 Emissions." E. Çiftyürek, K. Sabolsky, and E. M. Sabolsky, Materials Science & Technology 2013, Quebec, Canada. **PRESENTATION**.

10) "Nano-Derived Microsenors for Monitoring Gas Species in Harsh-Environments." E.M. Sabolsky, Çiftyürek, C. Wildfire, K. Sabolsky, J. Taub, K. Sierros, and T.H. Evans, 225th Electrochemical Society Meeting in Orlando, FL, May11-14, 2014; **INVITED PRESENTATION**.

Presentations of this Work

11) "Nano-derived Tungstate and Molybdate Oxides for the Sensing of H_2, H_2S and SO_2 at High Temperatures," E. M. Sabolsky, E. Ciftyurek, K. Sabolsky, 13th International Ceramics Congress in Montecatini Terme, Italy, June 8-13, 2014; **FUTURE PRESENTATION**.

Summary

- 10 Oral presentations in total
- 3 Invited oral presentations
- 1 Future oral presentation (in two weeks)
- 2 Ph.D. Dissertations (Engin Ciftyurek and Christina Wildfire)

Publications of this Work

1) E.M. Sabolsky, C. Wildfire, E. Çiftyürek, and K. Sabolsky, “Nano-Derived, Micro-Chemical Sensors for High-Temperature Applications”, Published in ECS Transactions, 45 (3) 495-506 (2012).

2) E. Çiftyürek, K. Sabolsky, and E. M. Sabolsky, “Platinum Thin Film Electrodes for High-Temperature Chemical Sensor Applications.”, Published in Sensors and Actuators B: Chemical, 181, 702-714 (2013).

3) C. Y. Wildfire, E. Çiftyürek, K. Sabolsky, and E. M. Sabolsky, “Fabrication and Testing of High-Temperature Nano-Derived Resistivity-Type Microsensors for Hydrogen Sensing”, Published to J. Electrochem. Soc. 161 [2], B3094-B3102 (2014).

4) C.Y. Wildfire, E. Çiftyürek, K. Sabolsky, and E. M. Sabolsky, “Investigation of doped-gadolinium zirconate nanomaterials for high-temperature hydrogen sensor applications.”, Published to J. Materials Science, 49 [14], 4735-4750 (2014).

5) E.M. Sabolsky, C. Wildfire, E. Çiftyürek, and K. Sabolsky, “Nano-derived Microsensors for Monitoring Gas Species in Harsh-Environments”, Published in ECS Transactions, 61 (2) 375-385 (2014).

6) E. Çiftyürek, K. Sabolsky, and E. M. Sabolsky “Functionally Gradient Zr-Pt Composite Thin Films for Stable High-Temperature Electrodes”, Submitted to Thin Solid Films, in May 2014.

2 more publications currently being prepared for H_2, H_2S and SO_2 sensing.

Background

Application of High-Temp Gas Sensors

- Industrial applications above 500˚C
- Special interest from DOE for harsh environment sensors (turbine engines, gasifiers, etc)
- Not for RT and ambient safety purposes
- Example of industrial environment

Slagging gasifier : (at 1315°C exit)

39.2% H_2, **40.3 % CO**, 0.11% CH_4, 17.3% CO_2, 0.87% H_2S+Sulfides, 0.41% H_2O, **0.78% O_2** *

*Ind. Eng. Chem. Res. 50 [3], 1674 (2011)

Background- Chemiresistive Sensors

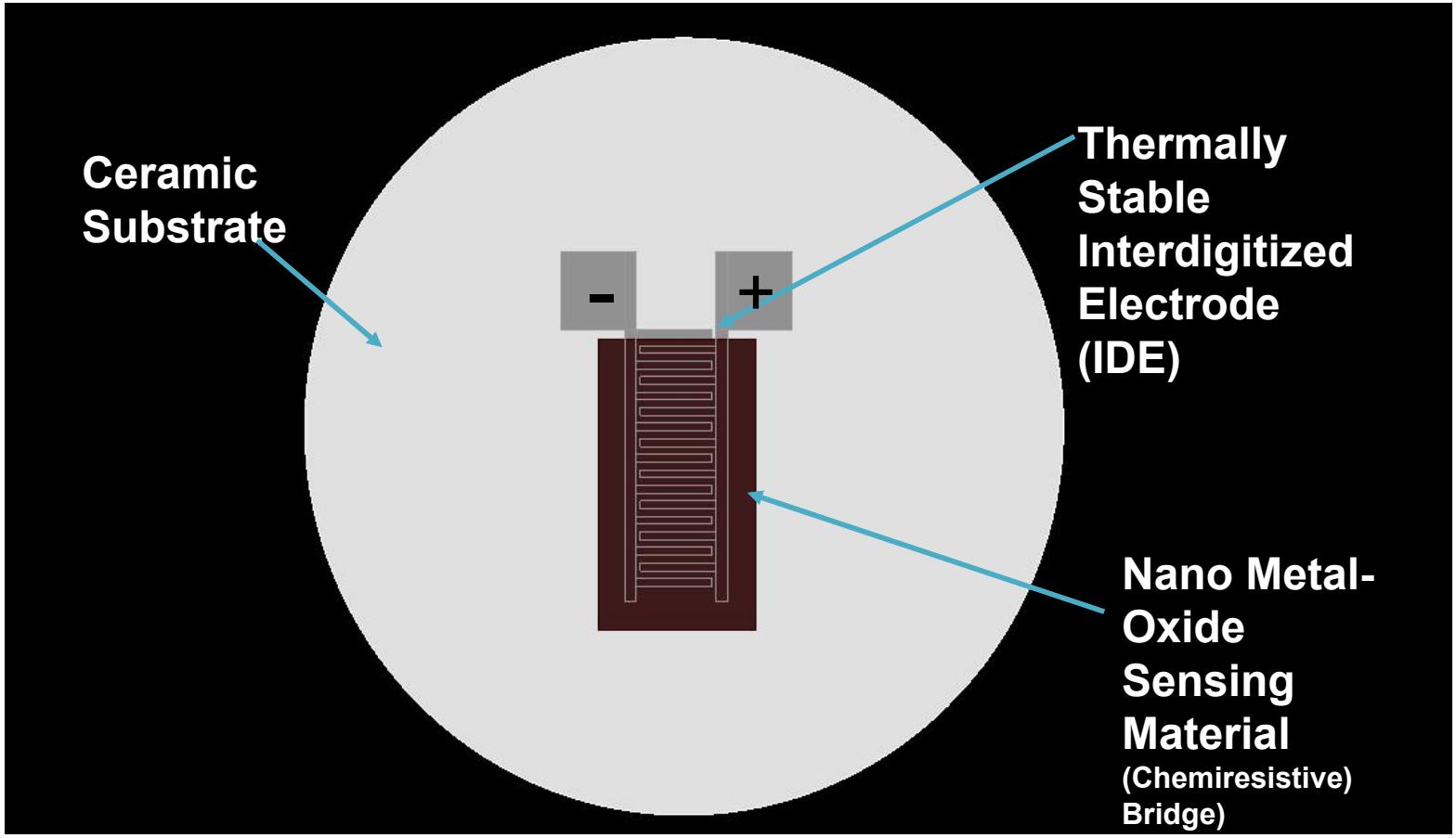

- Metal-oxide's shape, size, composition, and surface characteristics controls the selectivity and sensitivity.
- Nanomaterials provide ultra-high surface area which will enhance encounter of chemical species with sensing material.

Presented in Previous Reviews (2010-2013)

1) Hydrothermal processes for synthesis of ionic and mixed-conducting *zirconate, stannate, and titanate pyrochlores* (3-10 nm).
2) Resistor-type, macro-sensors of composite nanomaterials sense 500-4000 ppm H_2 (in air) at 600-1000°C *(where normal MOS degrade rapidly)*.
3) Nano-zirconate and SnO_2/zirconate nano-composites displayed enhanced stability.
   - From 0.792%/hr to 0.016%/hr (0.014 sensitivity for 500 ppm at 1000°C)
4) Initiated work on *Pt-based micro-IDEs that are stable to 1200 ℃*.
5) Initiated development of micro-casting and Dip Pen Nanolithography (DPN) processes for fabricating micro-sensor arrays.
6) Initiated work on sulfur sensing nanomaterial testing for SO_2 and H_2S.

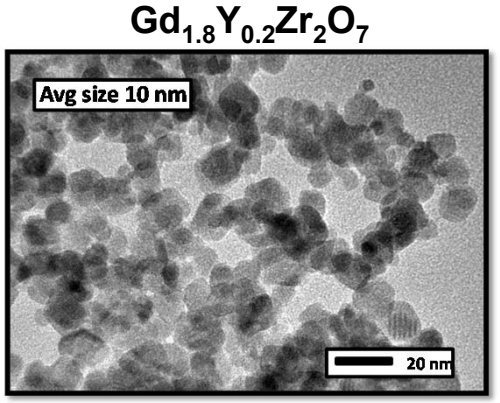

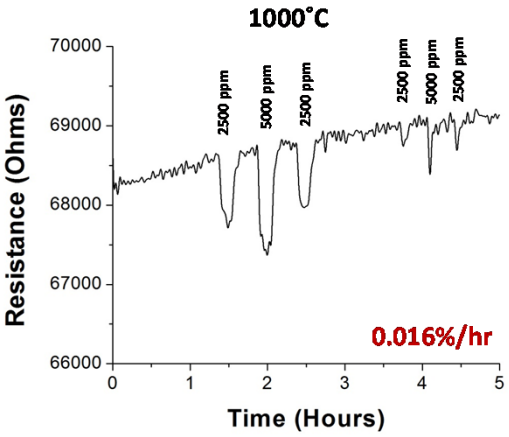

Challenges of Current Work Addresses:

1) **High-temperature stable micro-electrodes.**
   a. *Develop stable, DC sputtered micro-electrodes for specific sensing mechanism.*
   b. *Method for depositing and patterning potential complex microstructures and refractory metals.*

2) **High-temperature, stable, nanomaterials for sensing (H_2S, SO_2).**
   a. *Selective to species of interest.*
   b. *No reaction with other gas species in environment.*
   c. *Morphological stability at high temperature due to sintering and coarsening mechanisms (Driving Force $\approx 1/D^n$).*

3) **Method to micro-pattern particulate nanomaterials.**

High-Temperature Stable Electrodes (Inter-Digitized Electrodes, IDEs)

High temperature interdigitized electrodes (IDEs)

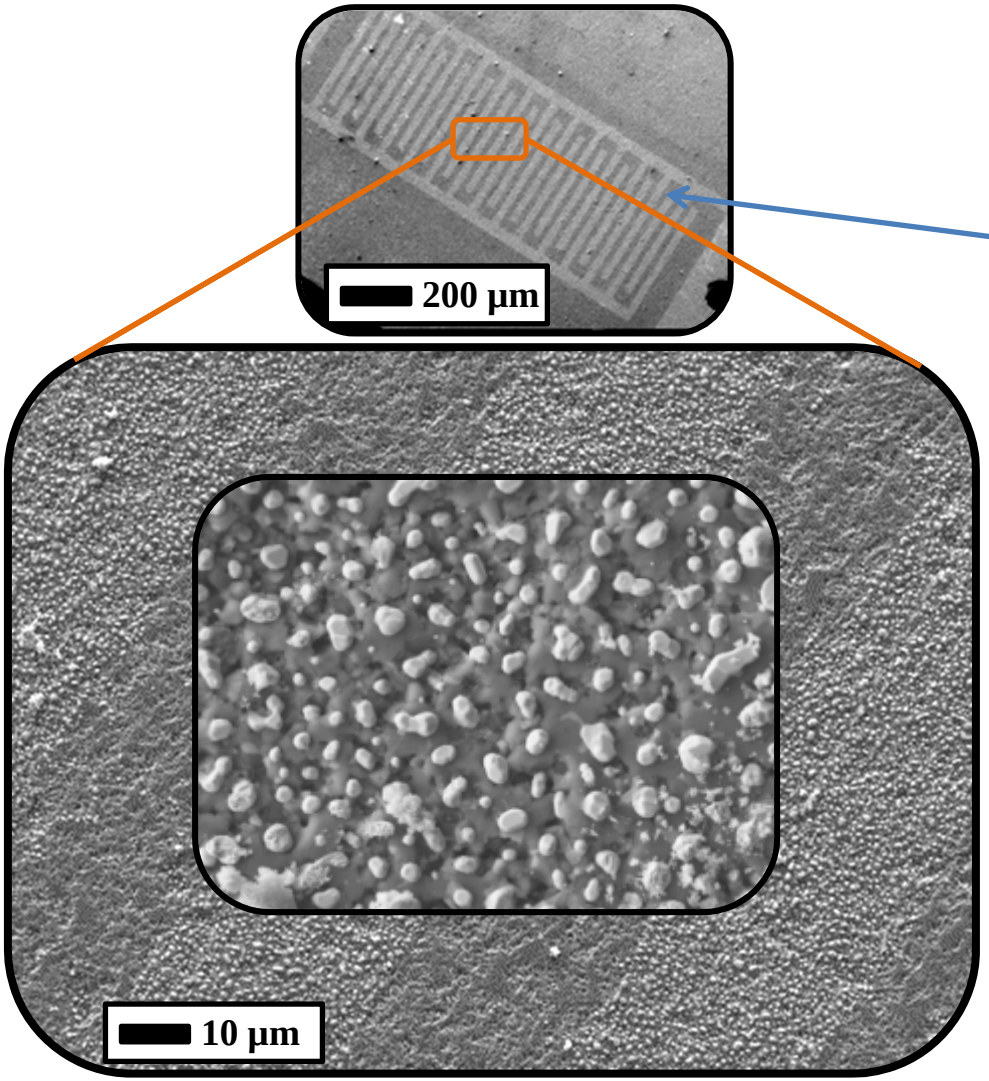

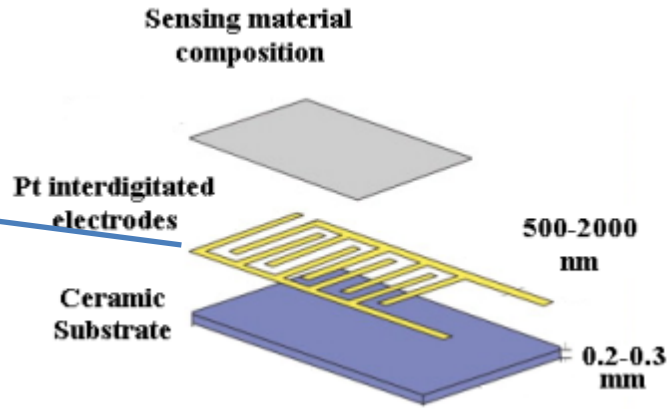

Current sensor technology is limited to operate at low temperature due to:

- Sensing material composition (stability, sensitivity, selectivity…)
- Processing (patterning of sensing material and electrodes)
- **Incompatible electrodes**

Percolation Lost!!!

Strategy to Stabilize IDEs

a) Using intermediate layer i.e. adhesion layer. → Surface tension

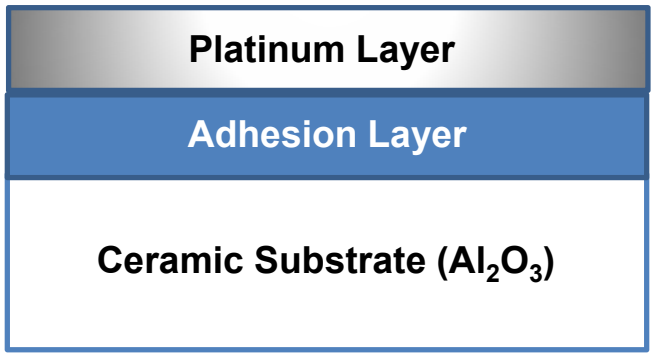

b) Using second phase precipitation. → Coarsening

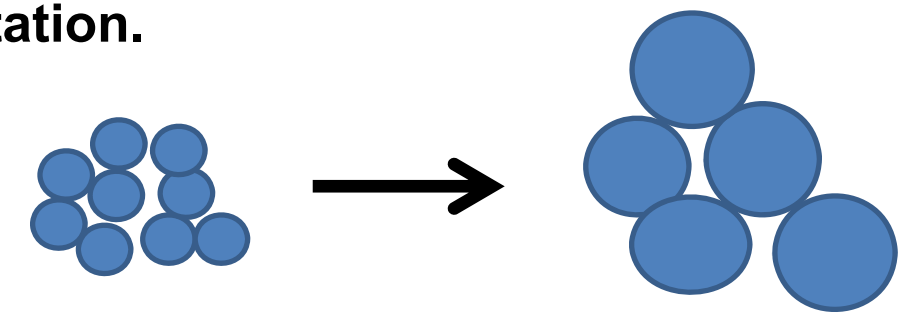

Coarsening/Sintering

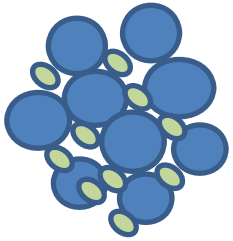

Grain Boundary Pinning Hinders Coarsening.

: Pt grain

: Second phase grain

Strategy to Stabilize IDEs

Schematic Representations

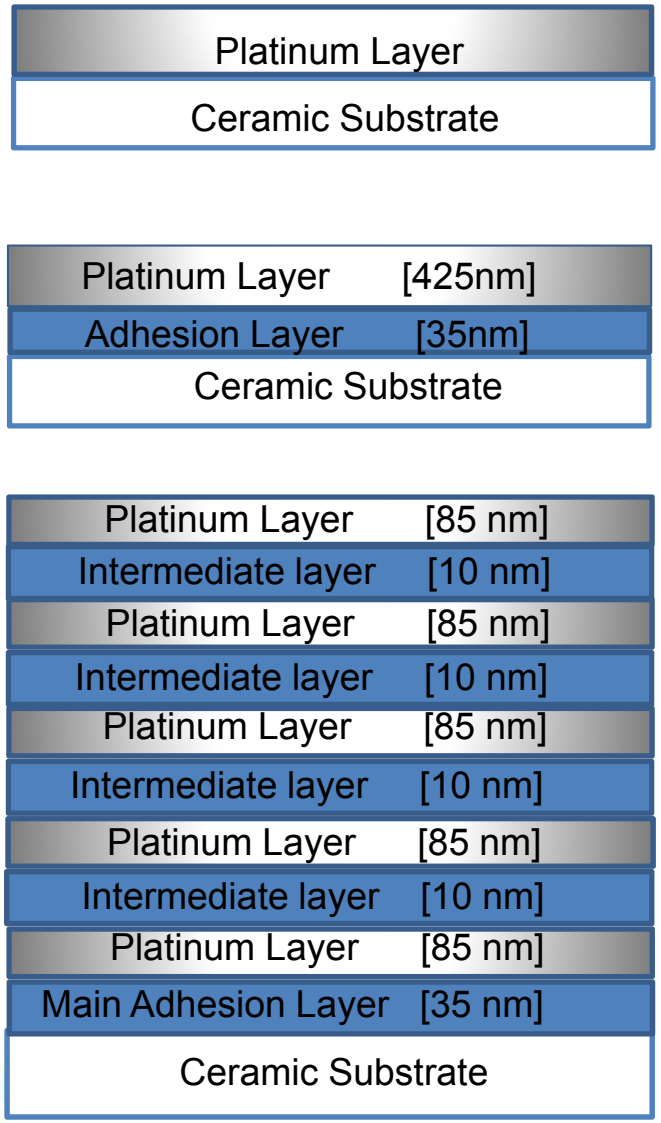

→ **Pure Pt**

BILAYER COATING ARCHITECTURES	
Titanium	Ti+Pt
Tantalum	Ta+Pt
Zirconium	Zr+Pt
Hafnium	Hf+Pt

MULTILAYER COATING ARCHITECTURES	
Zirconium	L-Zr+Pt
Hafnium	Hf+L-Zr+Pt

Summary: IDE Stabilization

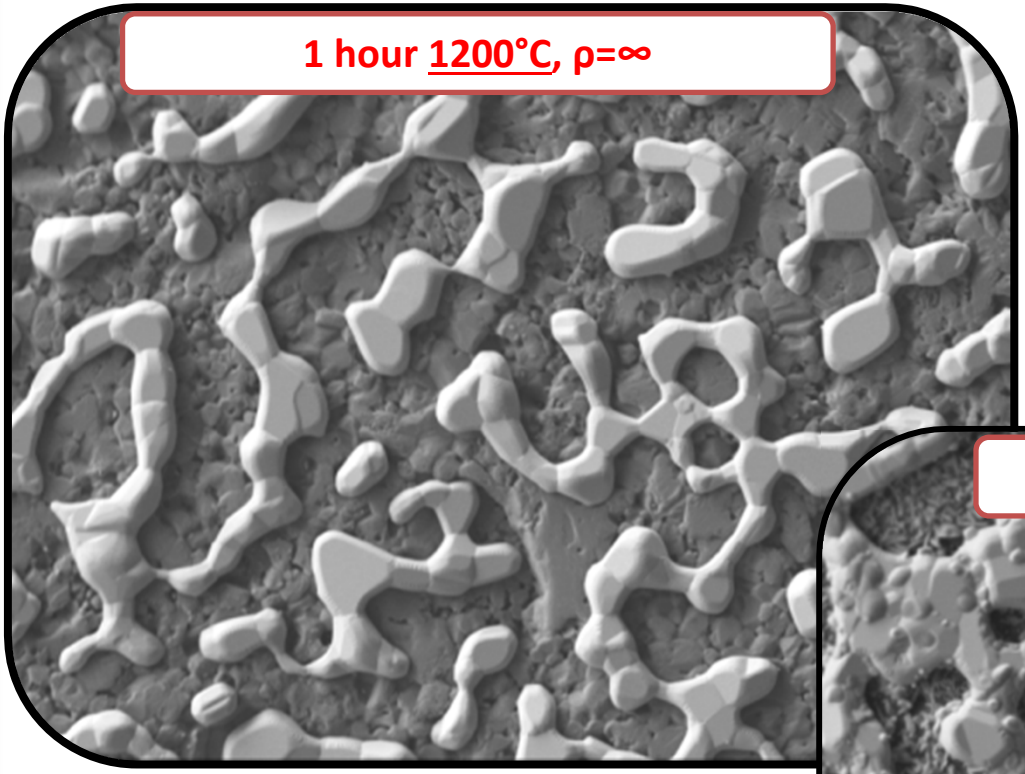

Ti or Ta adhesion layer + Pt layer

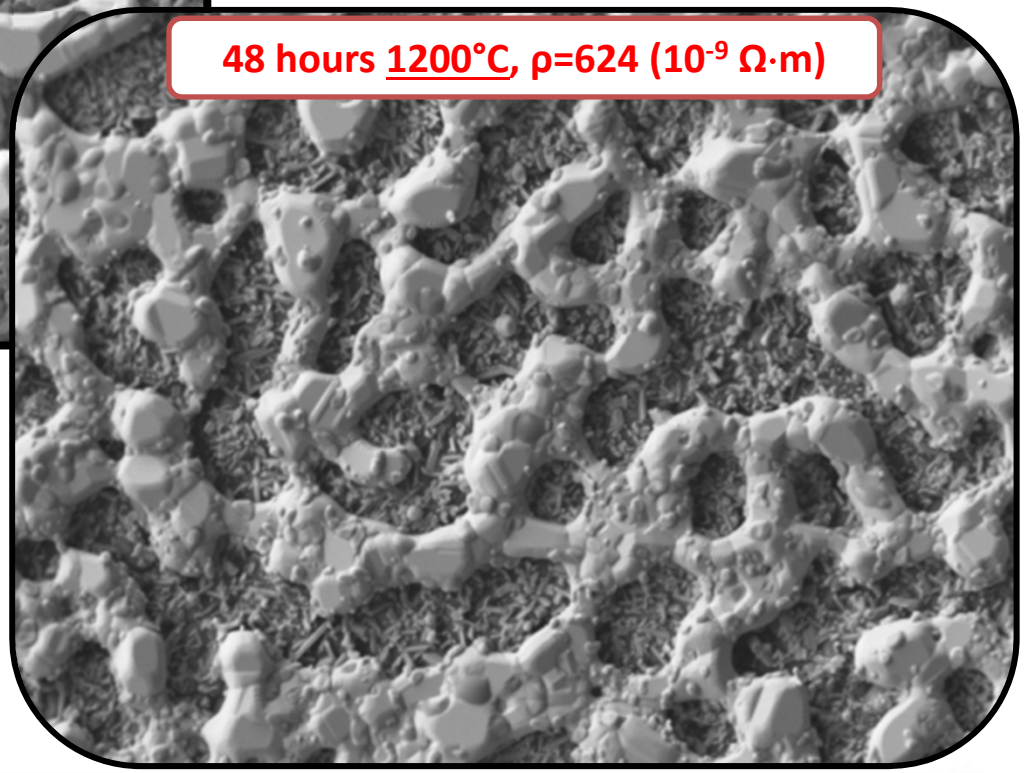

Hf adhesion layer + Zr+Pt composite

Summary: IDE Stabilization

Issue with Layer-by-Layer Electrode:

1) **Time consuming to deposit multiple layers.**
2) **Co-sputtering or solid-solution deposition requires specialized targets and equipment.**

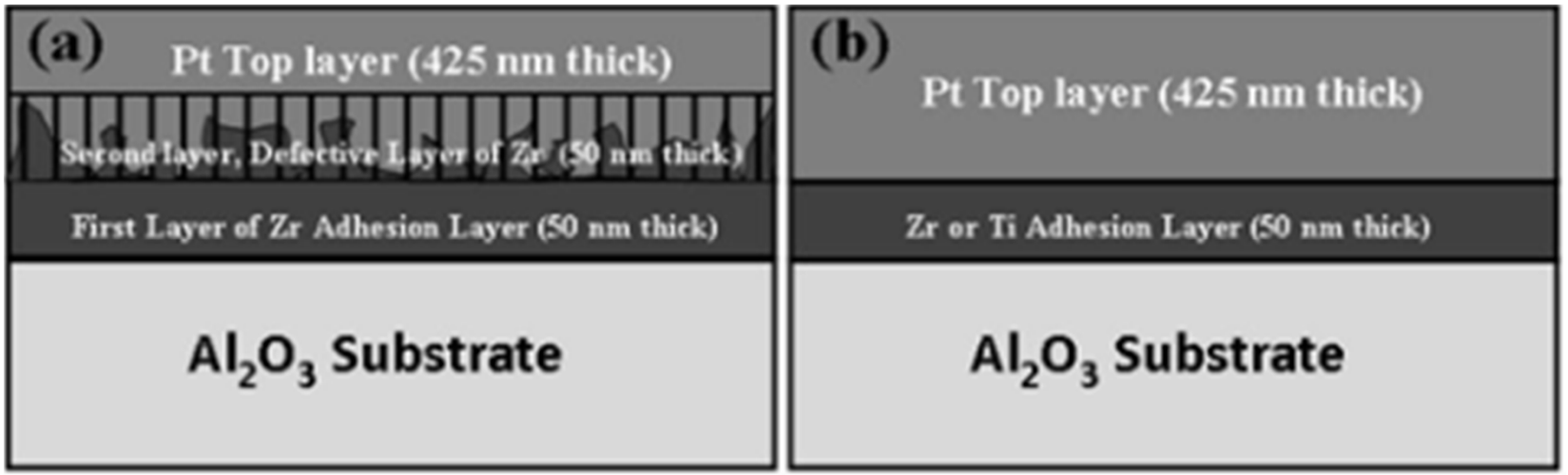

In order to access a similar grain-pinning strategy; *alternative approach; Pt with double zirconium adhesion layer,*

(a) Alternative approach, double layer, Zr/Zr+Pt/Pt
(b) Conventional Zr/Pt

High-temperature Functional Interdigitized Electrodes (IDEs)

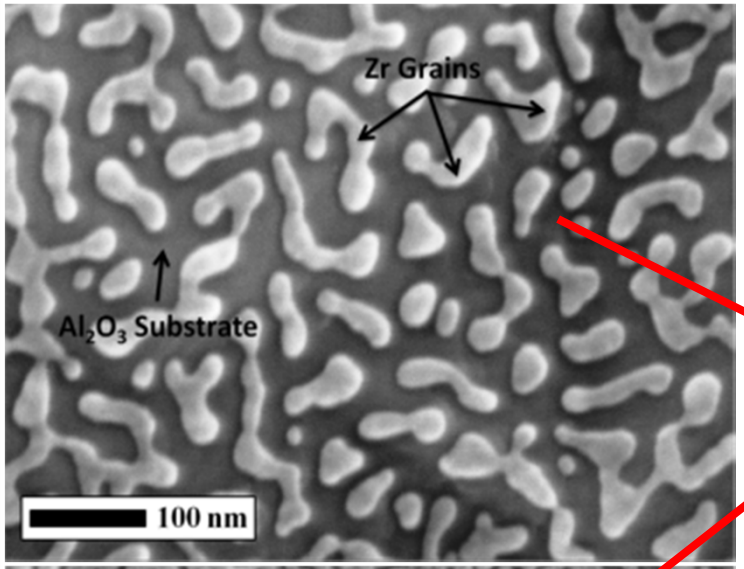

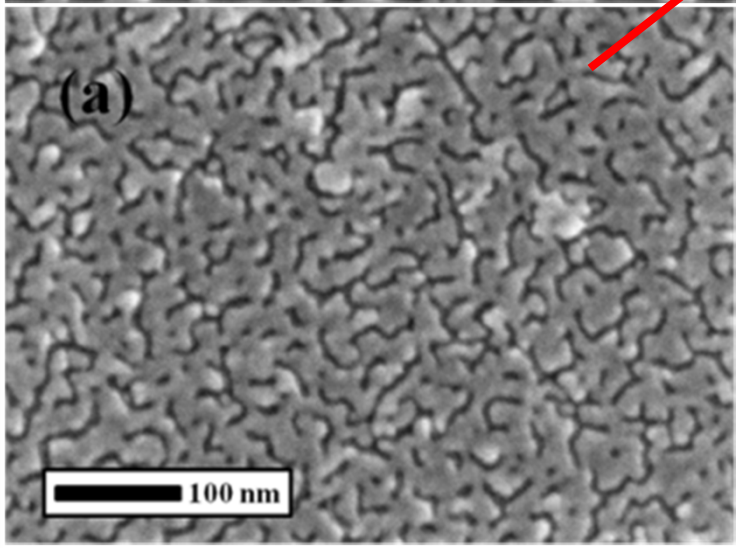

In order to access a similar grain-pinning strategy; ***alternative approach; Pt with double zirconium adhesion layer,***

(a) Alternative approach, double layer, Zr/Zr+Pt/Pt
(b) Conventional Zr/Pt

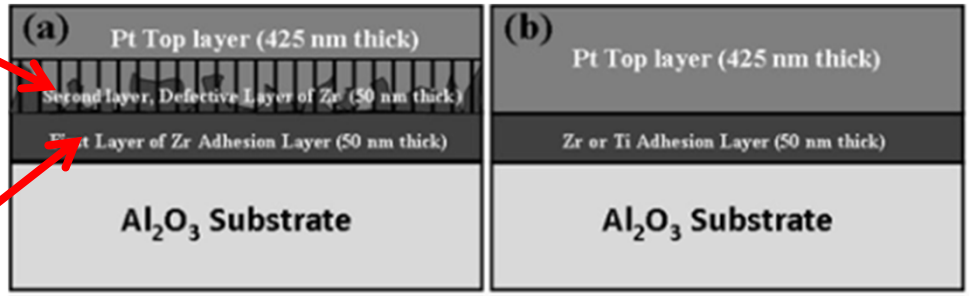

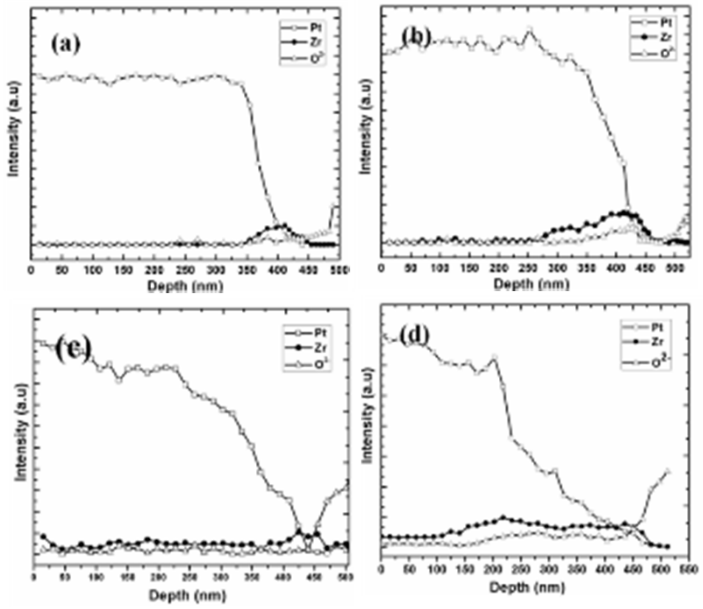

XPS depth profiling of

as-deposited
(a) Zr/Pt
(b) Zr/Zr+Pt/Pt and

annealed 1h at 1200°C
(c) Zr/Pt
(d) Zr/Zr+Pt/Pt thin films.

*Platinum-Zirconium Composite Thin Films Electrodes for High-Temperature MEMS Applications, E.Çiftyürek, K.Sabolsky, E.M. Sabolsky, JMEMS, 2013.

High temperature interdigitized electrodes (IDEs)

a) As-deposited **Zr+Pt electrode**.

b) Zr+Pt electrode after 1200°C, 15 h inert atmosphere annealing treatment. Inset shows the destruction of film continuity.

c) As-deposited **F-Zr+Pt electrode**.

d) F-Zr+Pt electrode after 1200°C, 15 h inert atmosphere annealing treatment. Inset shows the highly percolated Pt network.

Electrical Resistivity of Pt Composite Coatings (10^{-9} Ω·m)

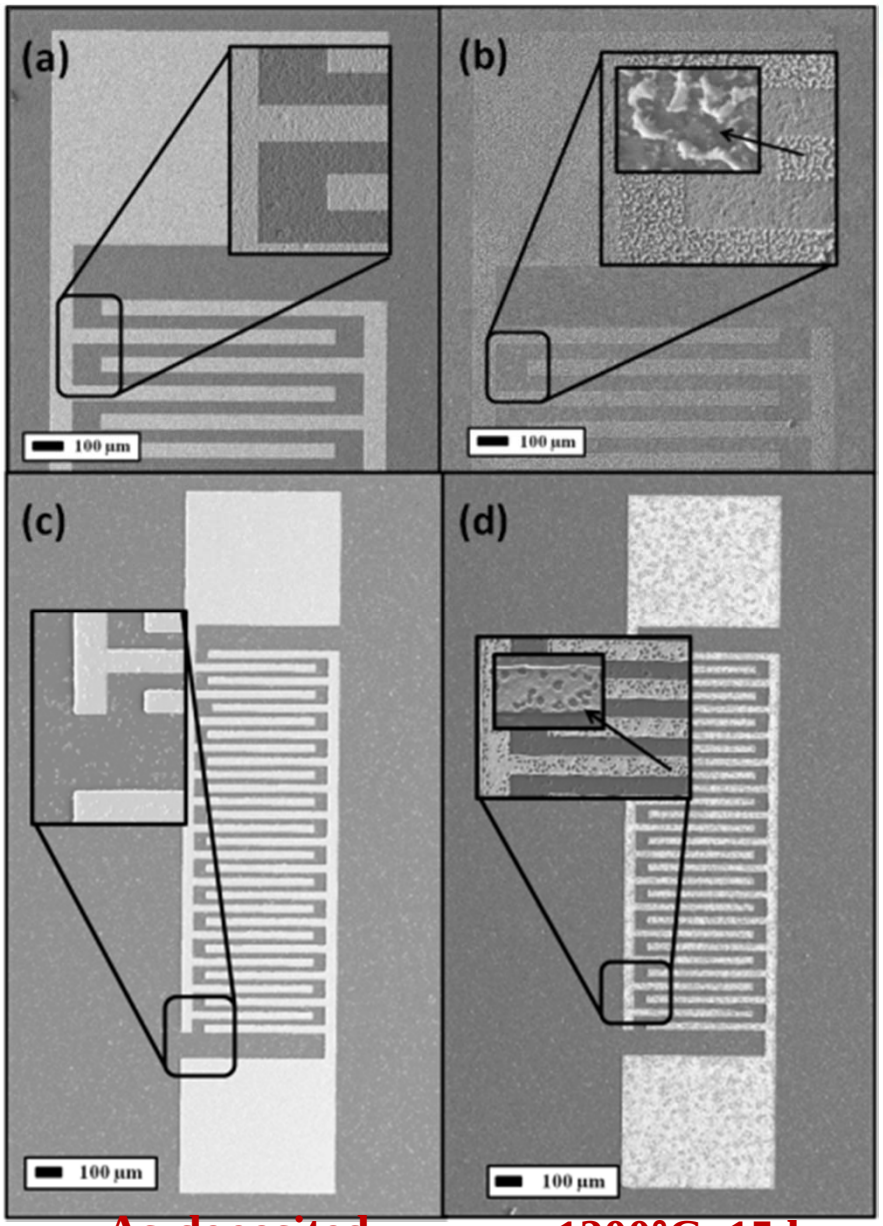

Nano-Derived Sensing Materials And Testing

Background-Sensing Materials for SO_2

Chemiresistive and Potentiometric and very limited number SAW devices.

Chemiresistive Type
WO_3 thick/thin film with different deposition methods
WO_3 with different noble metal loadings (Pt, Pd, Au, Ag)
TiO_2, V_2O_5 modified WO_3 and loaded with Au
NASICON-V_2O_5/WO_3/TiO_2 and/or decorated with noble metals

WO_3

Potentiometric Type
Na_2SO_4–$BaSO_4$–Ag_2SO_4
YSZ-LiSO-MgO
Li_2SO_4–$BaSO_4$
$(Al_{0.2}Zr_{0.8})_{10/19}Nb(PO_4)_3$
Li_2SO_4–doped $La_2O_2SO_4$
NASICON, ß-alumina and YSZ
$K_2SO_4Li_2SO_4$–Ag_2SO_4

Sulfates

Chemiresistive-type

- Most commercial product able to work <500°C.
- Not able to work at temperatures higher than 500°C.
- Simple structure, design and packaging, cheap.

Background-Sensing Materials for H_2S

Chemiresistive/Potentiometric Type
Fe_2O_3-$Fe_2(MoO_4)_3$
$Cr_{2-x}Ti_xO_3$
$La_{0.7}Pb_{0.3}Fe_{0.4}Ni_{0.6}O_3$
$CdIn_2O_4$
Ferrites

Ferrites

*S. K. Pandey *et. al.*, Trends in Analytical Chemistry, Vol. 32, 2012

- Literature related to H_2S larger than that of SO_2.
- Most of the works again devoted to the various types of **transition metal oxides (TMOs)** compounds, 25°C to 300°C.
- Ferrite sensitivities are typically lower in the range of (0-10%) even at temperatures between 100-400°C.

Original Sensing Compositions of Interest

- WO_3 shows *high affinity for sulfur compounds*, but unstable at high temperatures.
- ***Ternary tungstates and molybdates*** , wide band gap oxide-semiconductors (4-5 eV).
- Tungstates and molybdates display microstructural, chemical and morphological stability at high temperatures (compared to WO_3 or MoO_3).

- WO_3
- WO_3 nano
- MoO_3
- MoO_3 nano
- $MgMoO_4$
- $NiMoO_4$
- $NiWO_4$
- Sr_2MgWO_6 (SMW)
- Sr_2MgMoO_6 (SMM)
- $SrMoO_4$
- $SrMoO_4$ nano
- $SrWO_4$

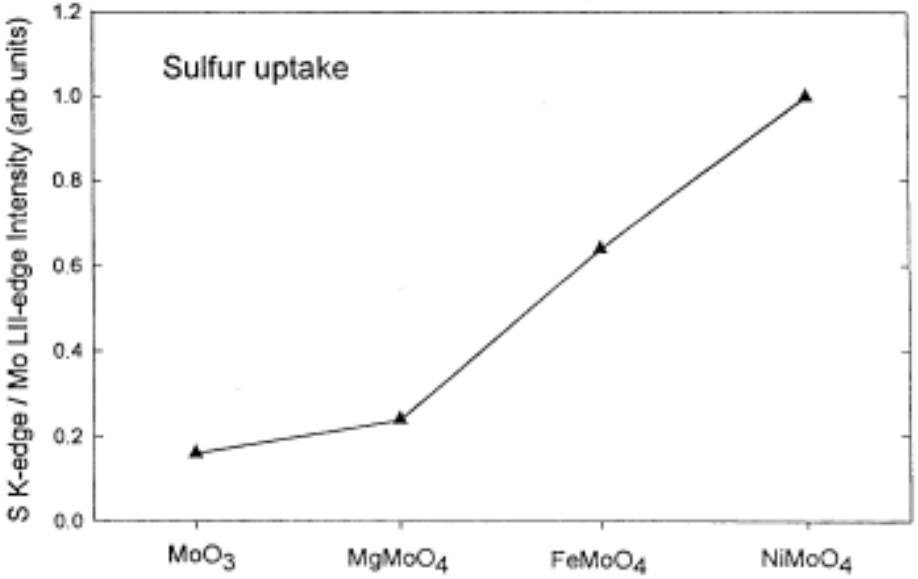

*J. A. Rodriguez, Catalysis Today, 2003

Synthesis of W and Mo oxides

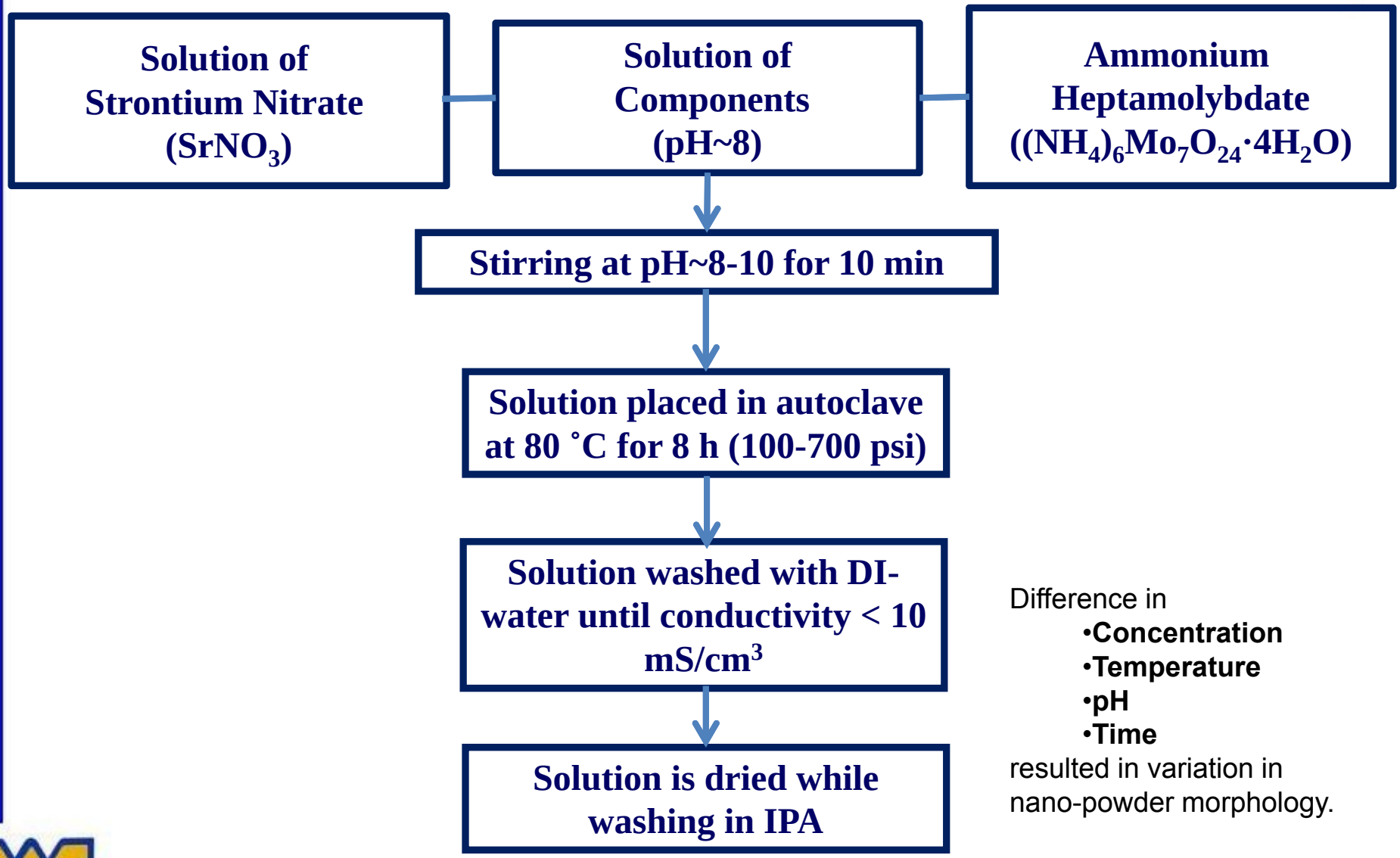

Difference in

- **Concentration**
- **Temperature**
- **pH**
- **Time**

resulted in variation in nano-powder morphology.

Sensing Nanomaterials Synthesized

- **Nano-materials with different morphologies were synthesized via hydrothermal route**

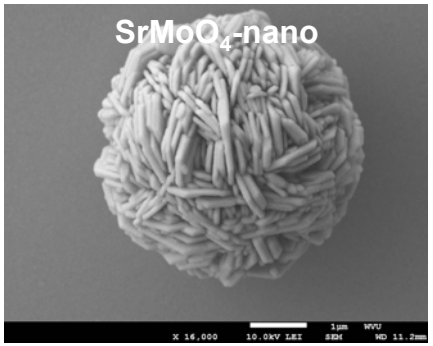

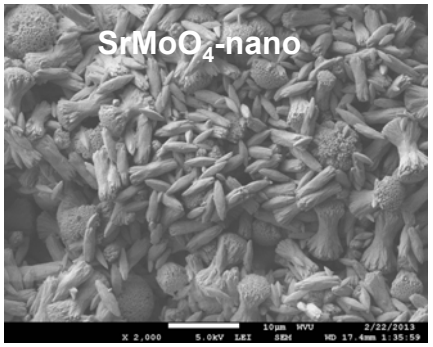

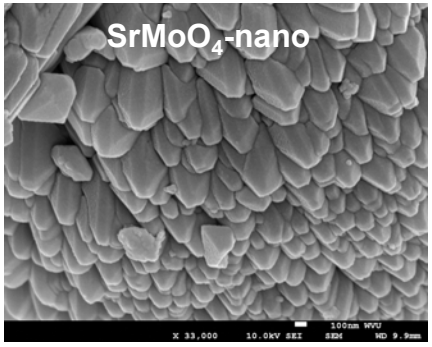

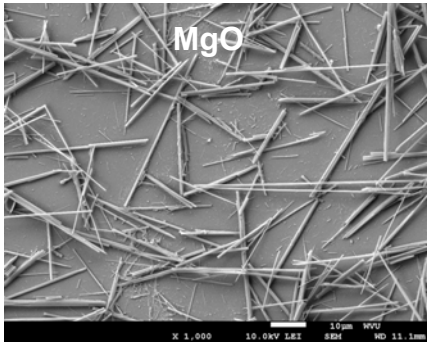

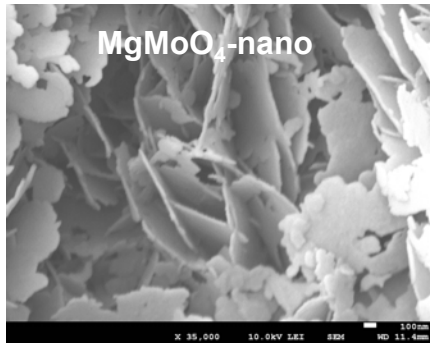

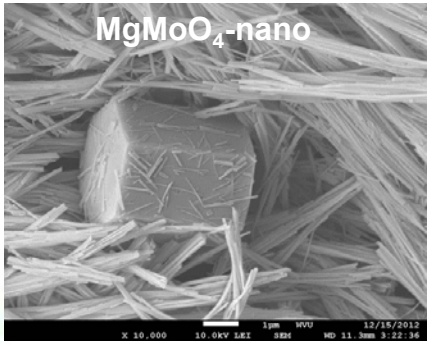

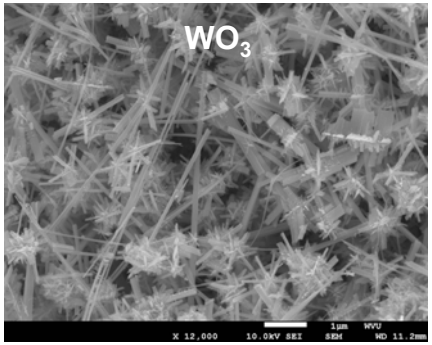

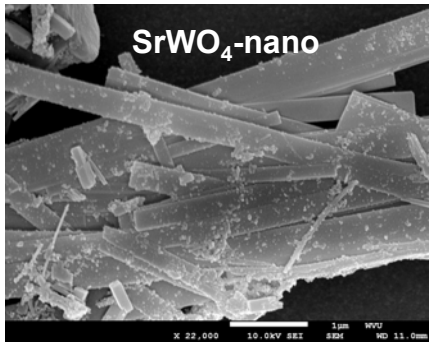

Sensor Testing Procedure

- Polished alumina substrates.
- Pt-IDEs screen-printed and annealed at 1200˚C.
- Sensing material printed onto electrodes and sintered at 1200˚C (~100 µm thick) .
- Total flow adjusted to 50 sccm with testing at 600, 800, 1000˚C
- Exposure to H_2, SO_2 and H_2S in N_2 atmosphere (various 1, 5 and 20% O_2).

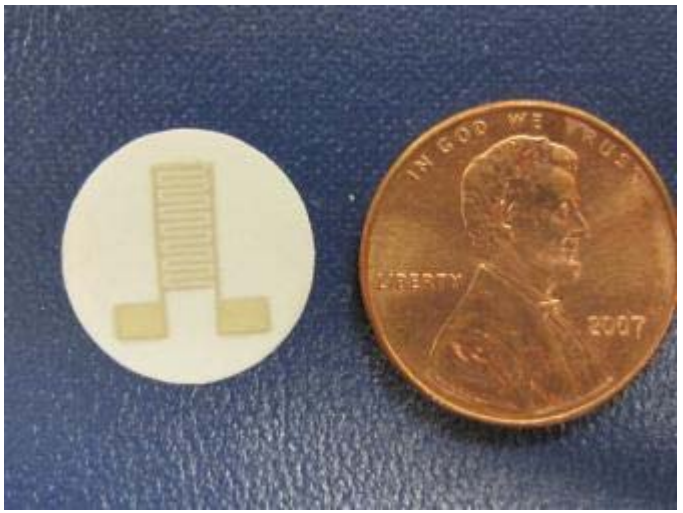

Screen-printed Macro Electrode
(250 µm finger spacing)

$$Sensitivty = S = \frac{R_{gas} - R_{base}}{R_{base}}$$

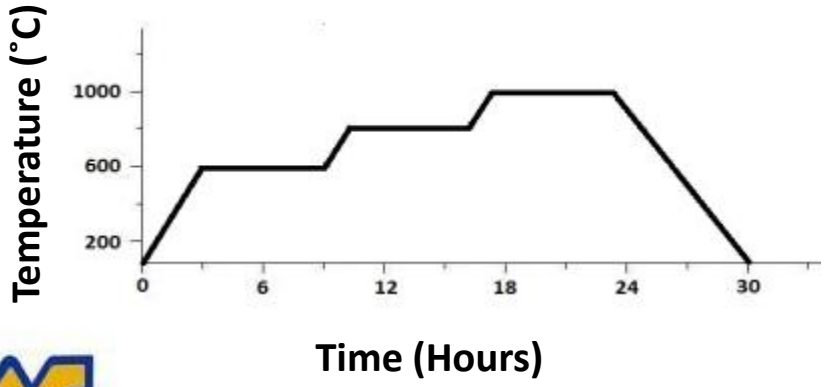

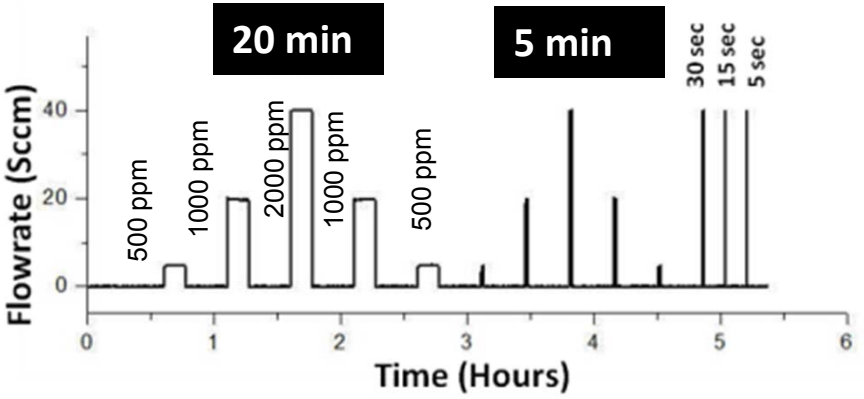

Initial Evaluation of Sensing Nanomaterials

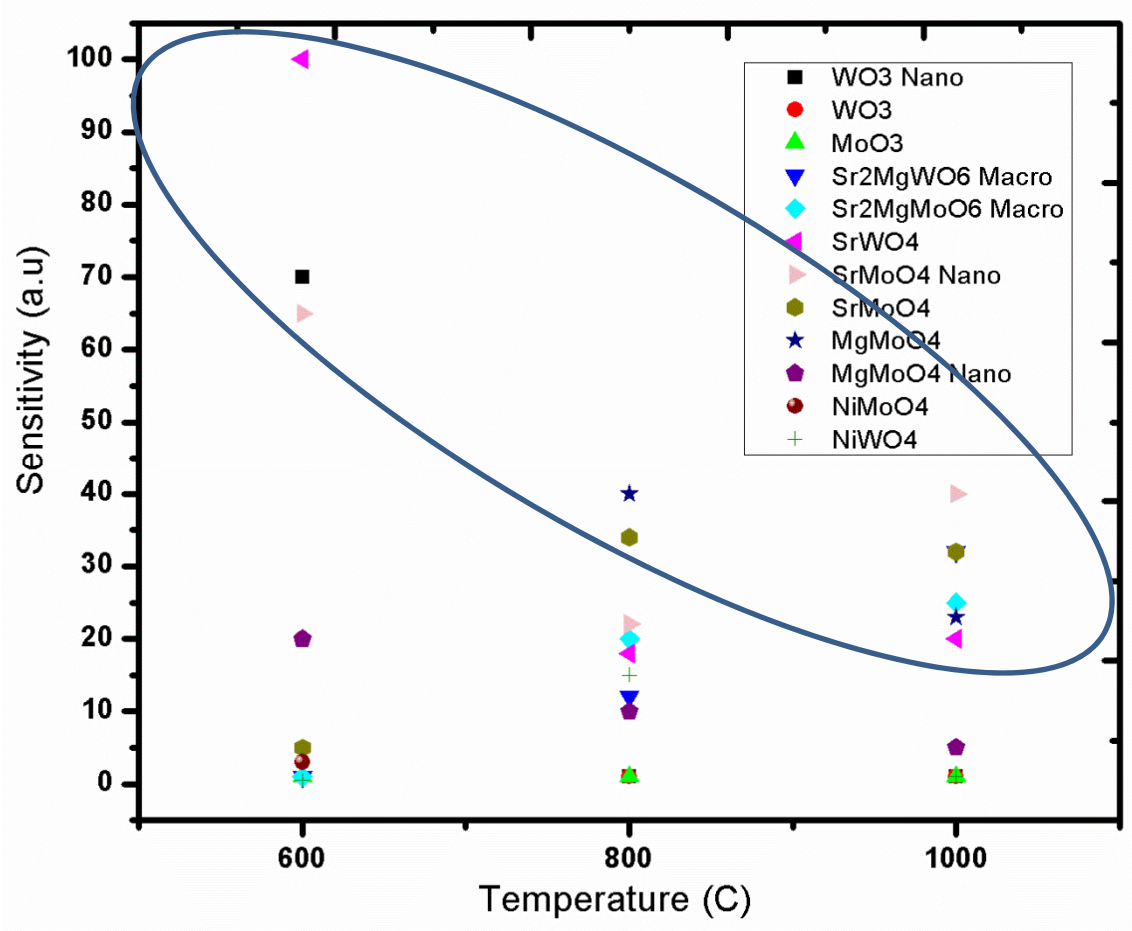

2000 ppm SO_2
1% O_2 (in N_2)
(Similar to gasifier)

•Nanomaterials were tested for stability response and recovery times.
•WO_3 (at low temp), $SrWO_4$ and $SrMoO_4$ show the highest sensitivity at high temperature.

Summary of Sensing Material Testing for SO_2

WO_3

- Reduction problem

$NiWO_4$

- Reduction problem

$SrWO_4$

- High sensitivity
- Cross-sensitivity problem

$SrMoO_4$

- Highest sensitivities at high temperature
- Lowest cross-sensitivities against CO and H_2
- Long term stability (100 h testing)

Characterization of Nano-WO_3 Sensing Materials

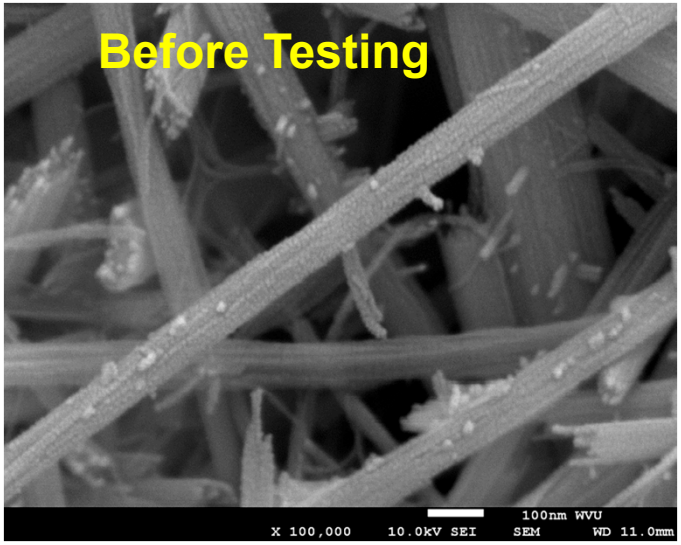

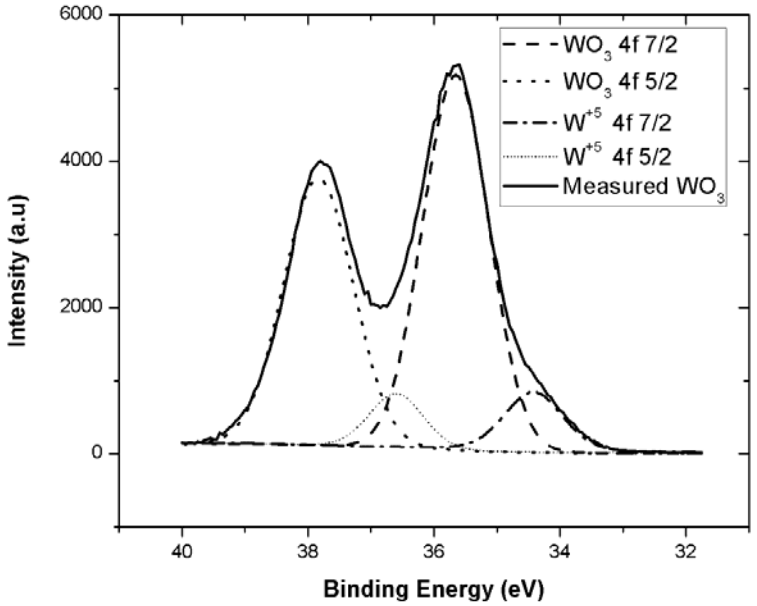

- 5-100 nm nano-rods
- W^{6+} are 35.67 and 37.85 and W^{5+} 34.46and 36.84 eV, color is light blue.
- 14.02% W^{5+} and 85.98% W^{6+} no other chemical state was detected.

1000°C

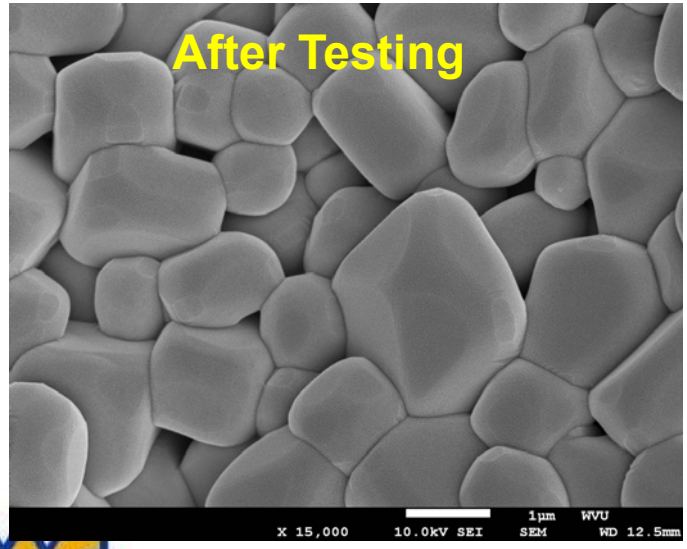

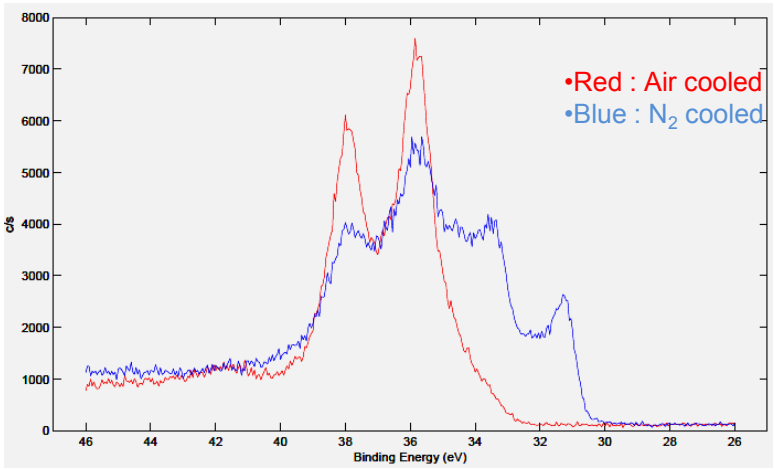

•XPS Analysis

SO_2 Sensing using Nano-WO_3 Materials

- N_2, 1%O_2, different concentrations of SO_2.

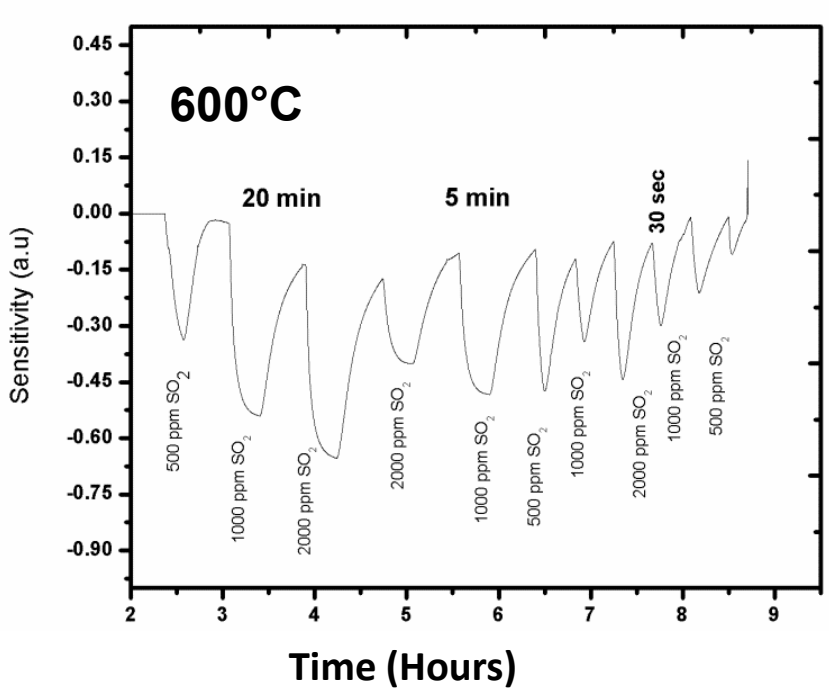

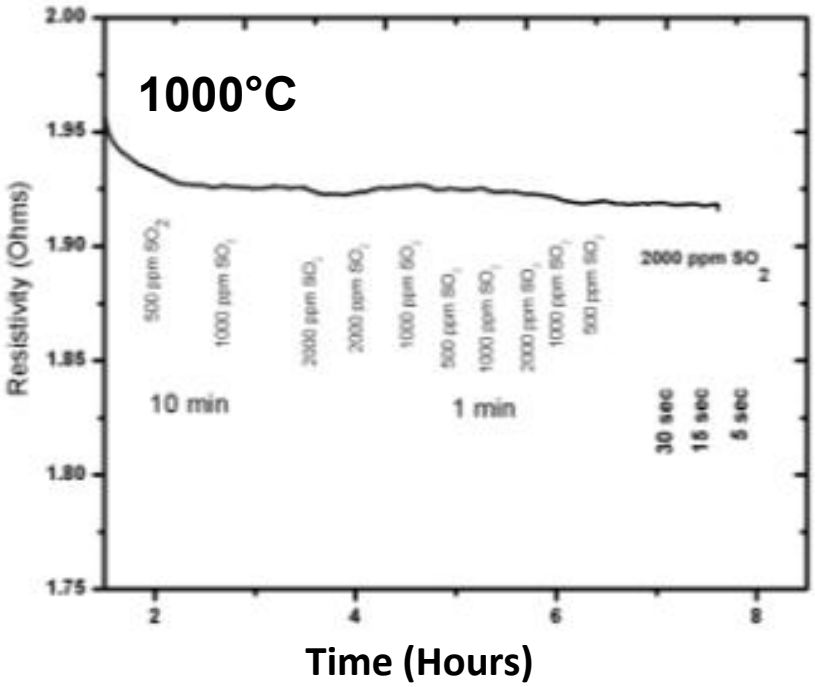

- Insensitive at 1000°C due to reduction of semi-conductor to metallic state

SEM Characterization of $SrMoO_4$ Sensing Materials

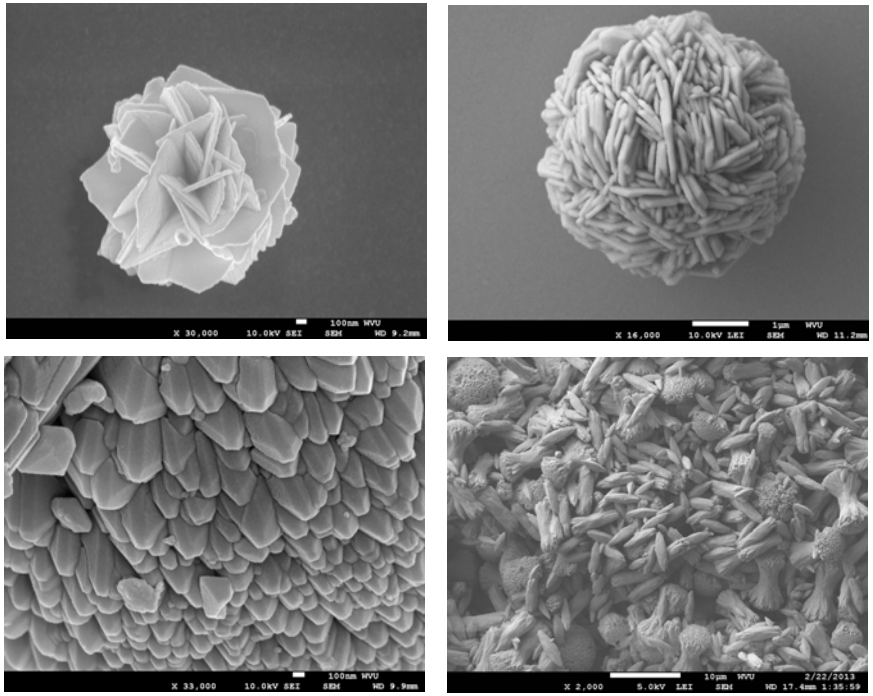

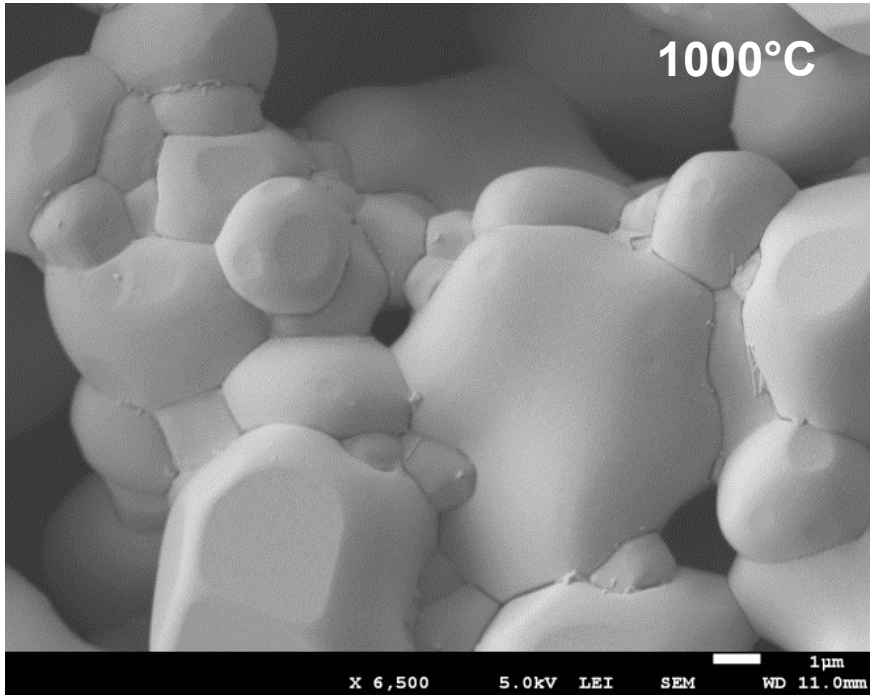

- As-synthesized $SrMoO_4$ powders with different morphologies, confirmed by XRD not included.

- $SrMoO_4$ powders with different morphologies after testing

SO_2 Testing of Nano-$SrMoO_4$ Sensing Materials

N_2, 1%O_2

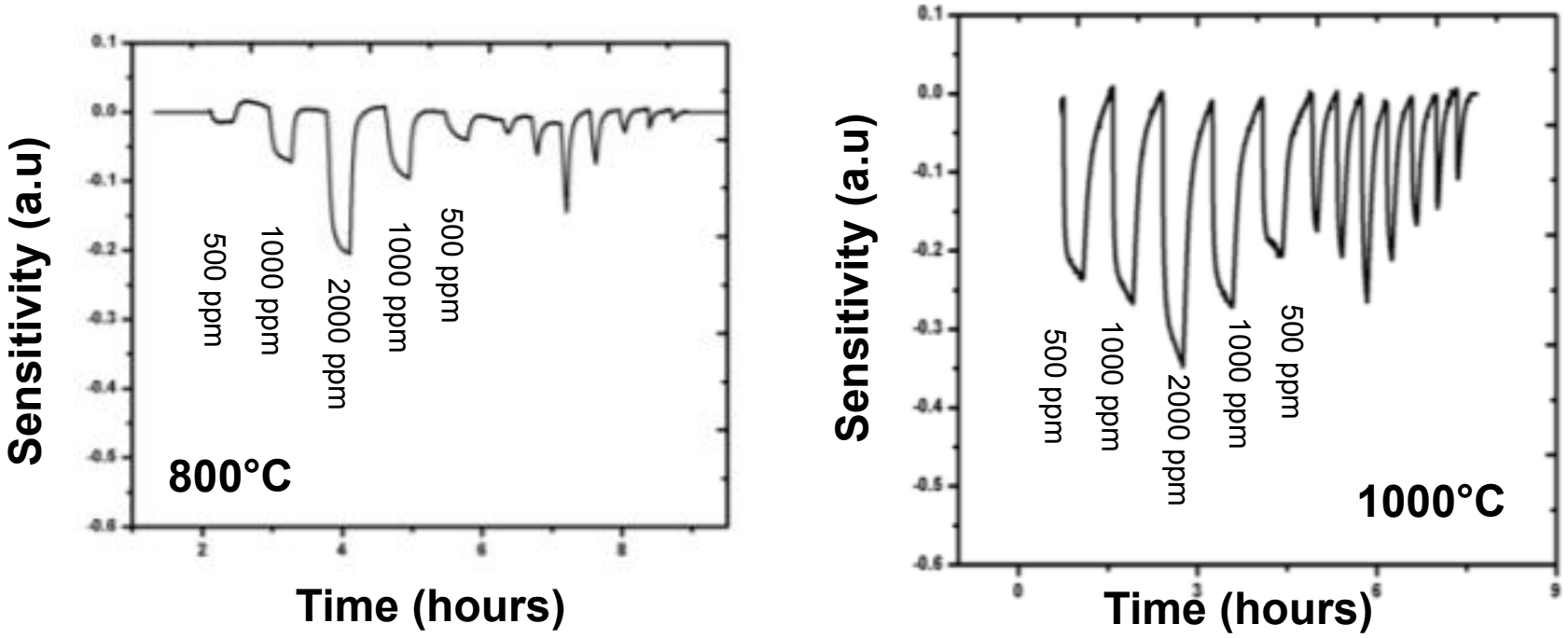

- High sensitivity even with coarsening of nano-particles.
- High sensitivity REGARDLESS of nano-particle morphology..

Cross-sensitivity Tests of Nano-$SrMoO_4$

H_2 concentration level is always two times than that of SO_2

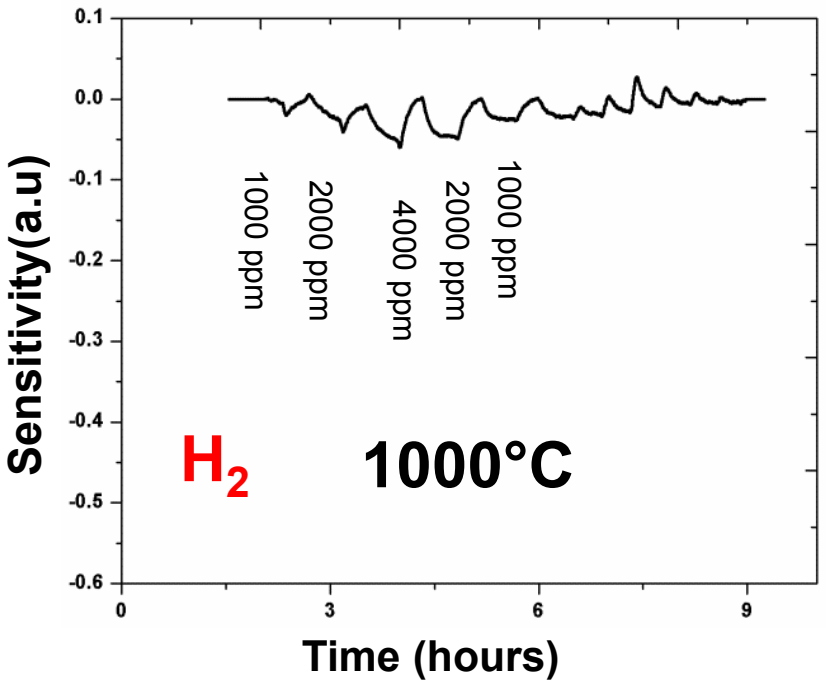

CO concentration level is two times than that of SO_2

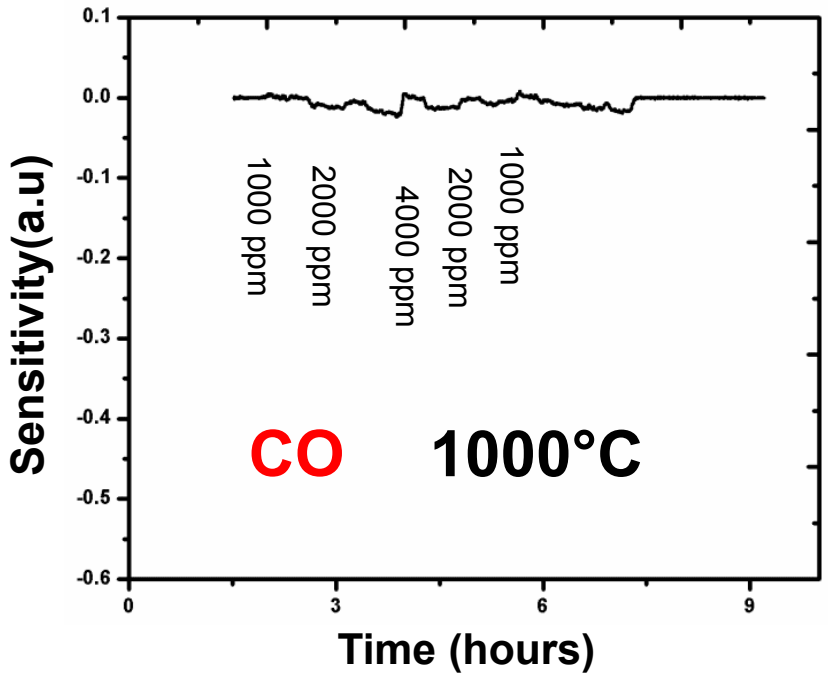

- **CROSS-SENSITIVITY TESTS SHOWED APPLICABILITY of nano-$SrMoO_4$ further.**

H_2S Sensing of Nano-$SrMoO_4$ Sensing Materials

N_2 with 1% O_2

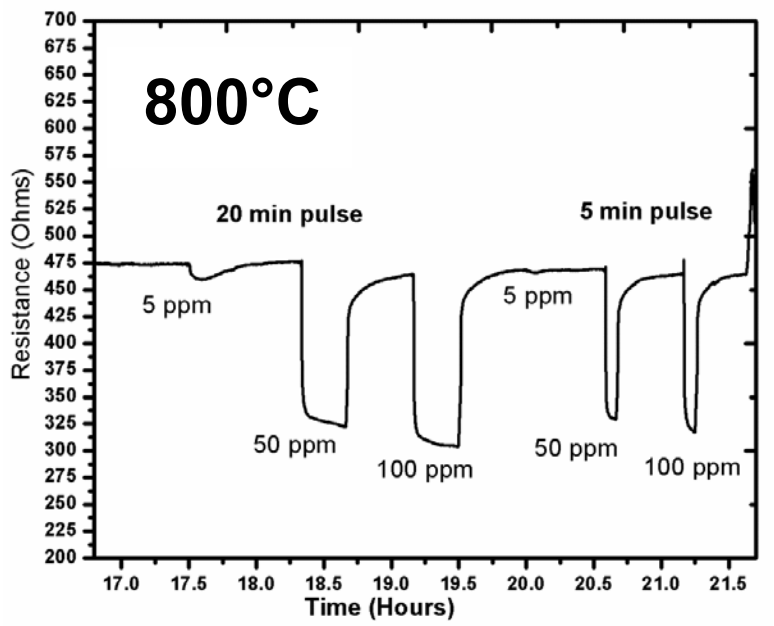

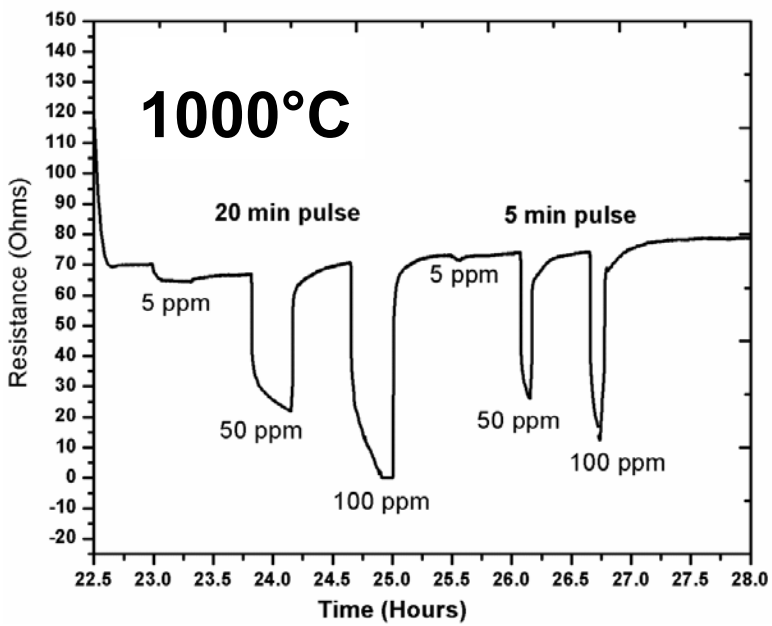

- Sensitive towards 5, 50, and 100 ppm H_2S at 800 and 1000°C
- N-type behavior
- Long term stability (48 h testing) test showed similar sensing behavior.

SEM Characterization of Nano-$SrMoO_4$ after Testing

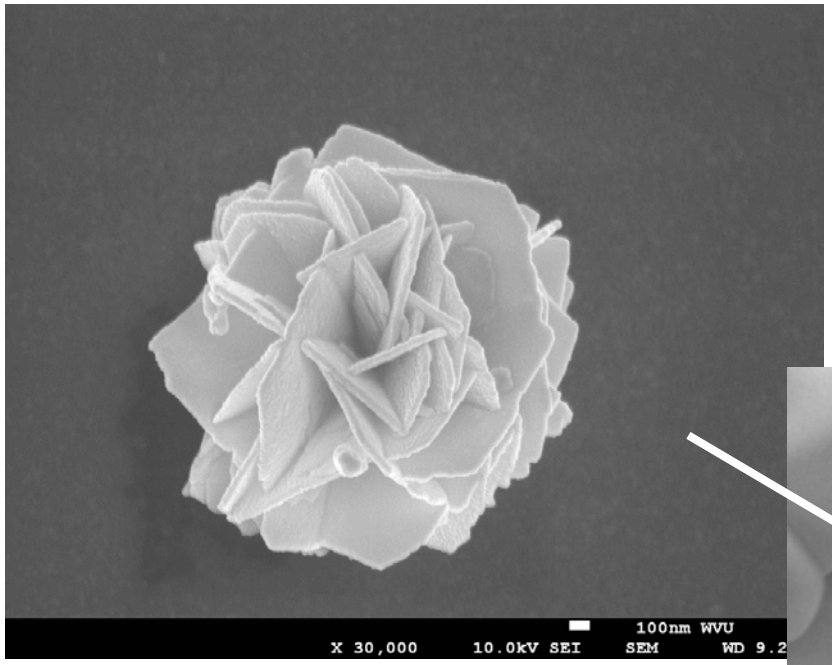

•Regardless of morphology (5 different morphology were tried) this is what happens at elevated temperature!!!

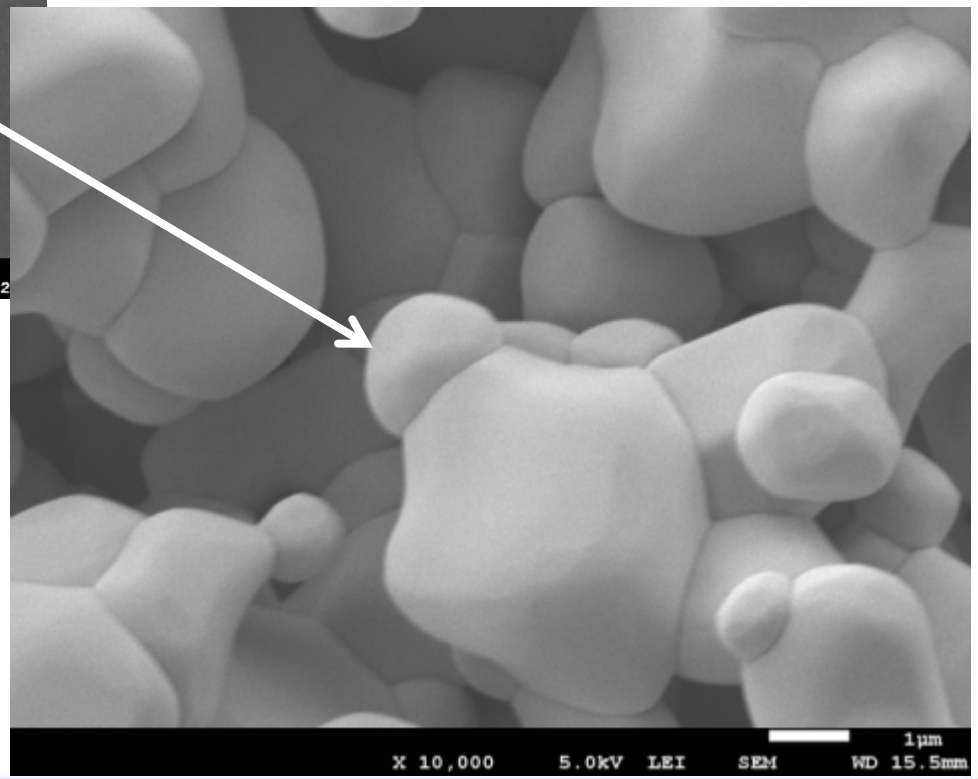

Solutions to Limit Coarsening of Nano-$SrMoO_4$

1. **Grain-pinning**

   - Zener Pinning: Benefiting from the influence of fine refractory-stabile particles on the movement of low and high angle grain boundaries by exerting a pinning pressure.

2. **Templated growth of $SrMoO_4$**

   - Deposit sensing material over a core refractory-oxide structure preferentially with epitaxial match.

SEM Characterization of Grain-pinning Strategy

1. Grain-pinning via nano-CeO_2

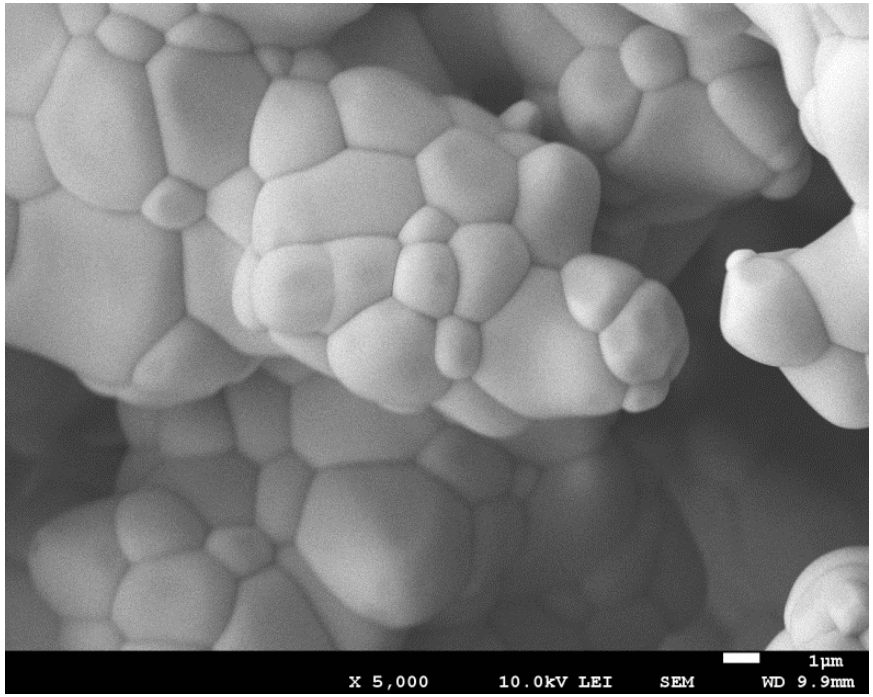

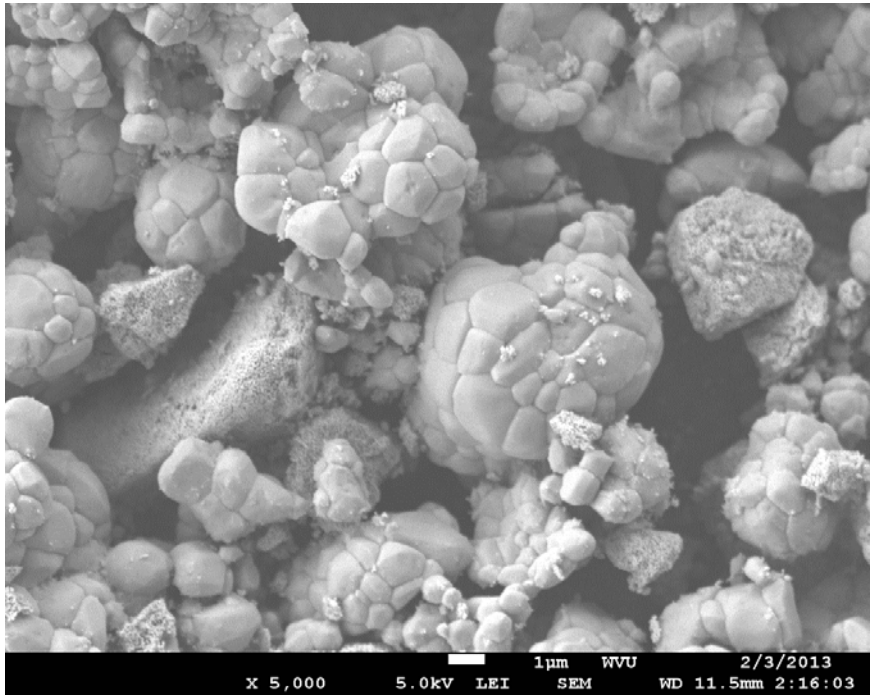

- Limited success !!!

SEM Characterization of Refractory Core Strategy

2. Templated growth of $SrMoO_4$ over a core refractory MgO.

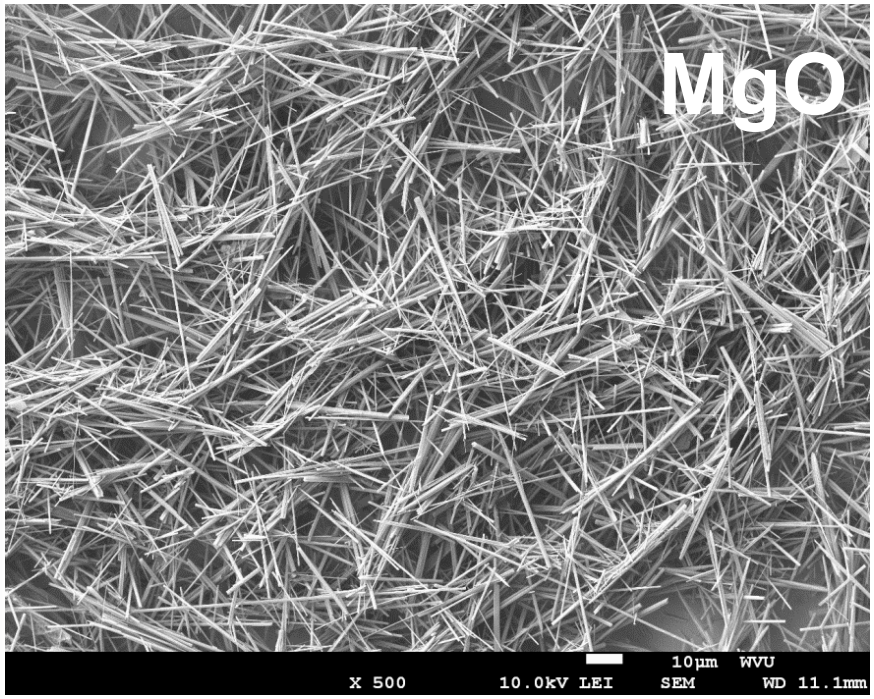

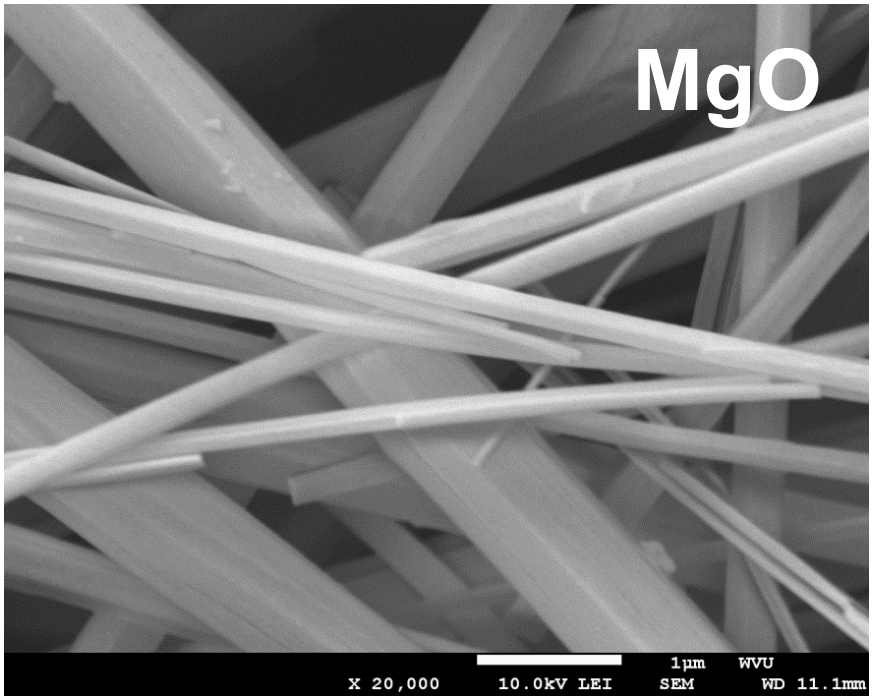

- **For this purpose, MgO nanorods were synthesized.**
  - MgO stable compound.
  - Epitaxial match with the final compound.

SEM Characterization of Refractory Core Structure and Nano-$SrMoO_4$

2. Template Growth, over a core refractory structure with nano-features.

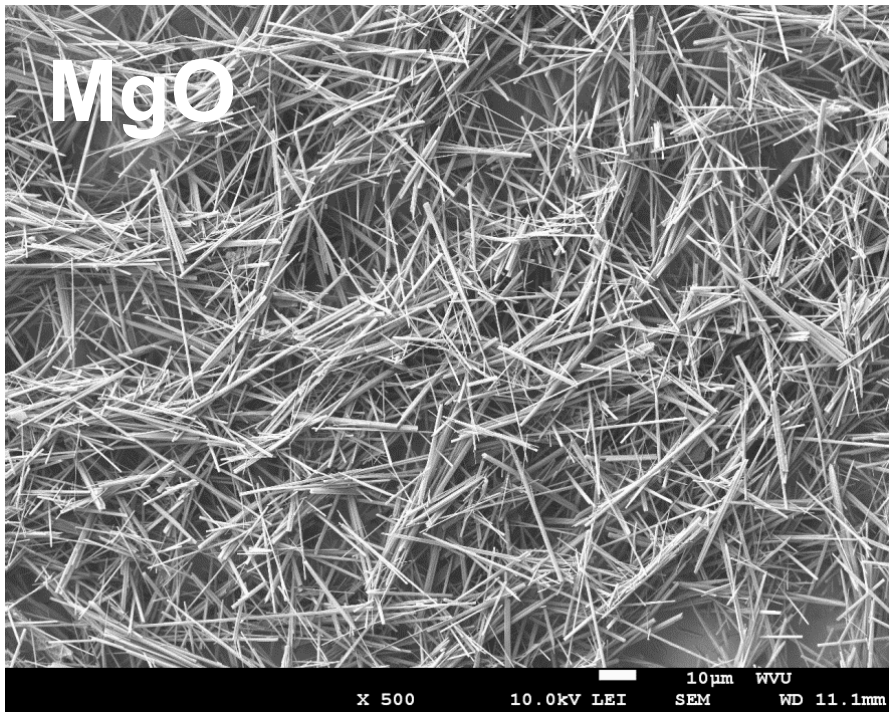

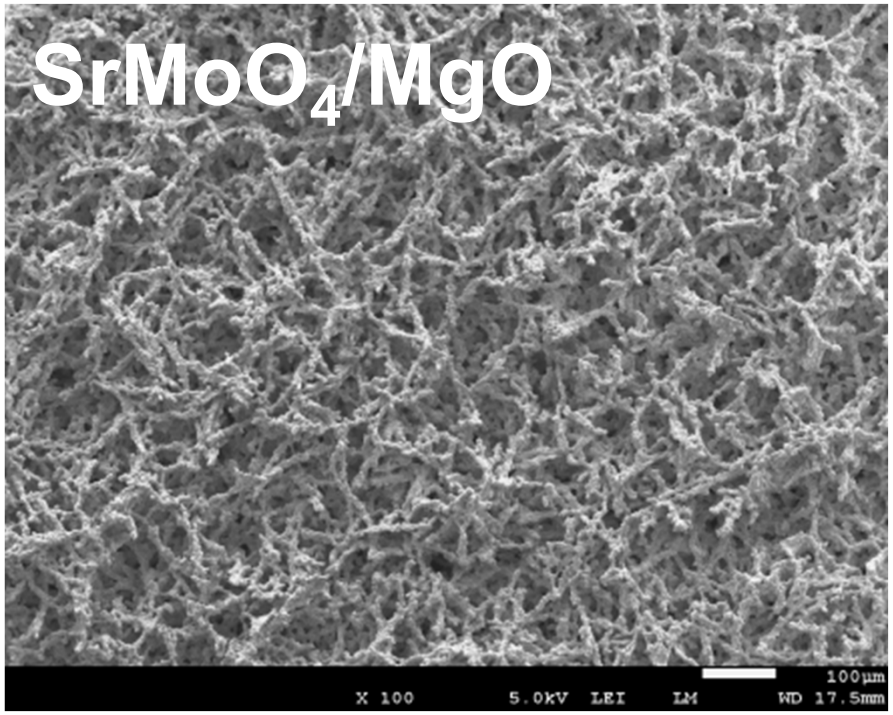

And tried grow ***$SrMoO_4$ over MgO, worked…***

SEM Characterization of Refractory Core Structure and Nano-$SrMoO_4$

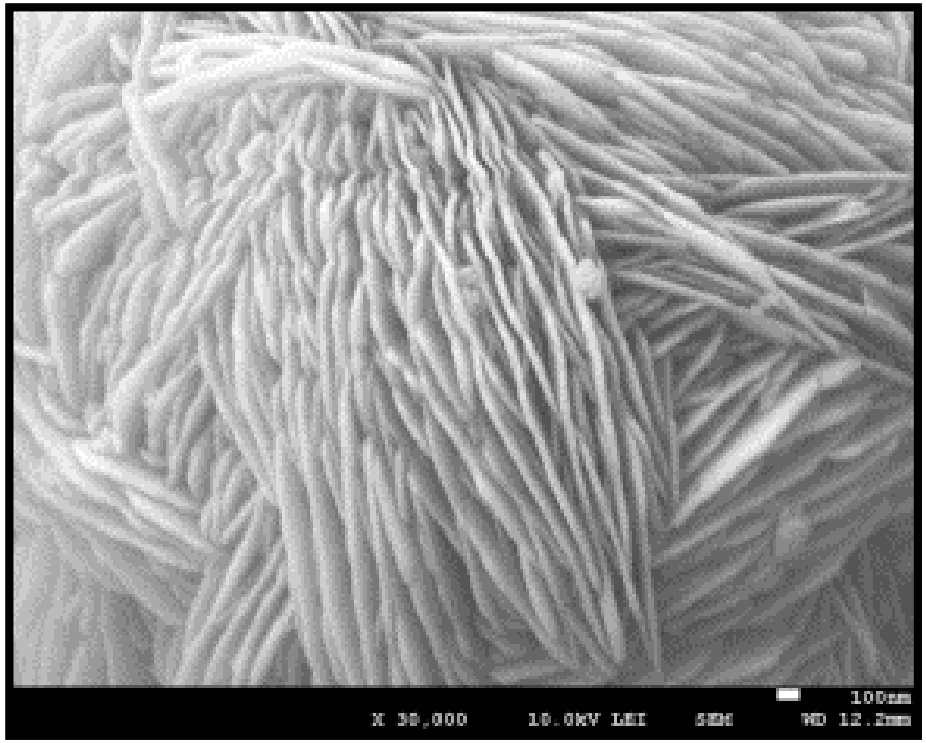

•High magnification SEM shows $SrMoO_4$/MgO presents nano features.

Nano-$SrMoO_4$ over MgO

SEM Characterization of Refractory Core Structure and Nano-$SrMoO_4$

5 h, 1000°C in air

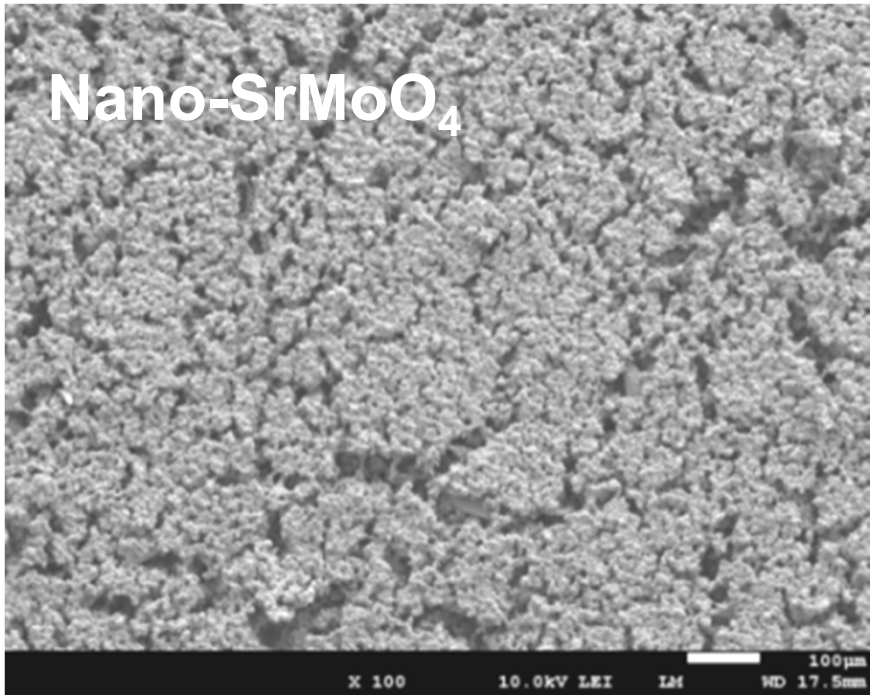

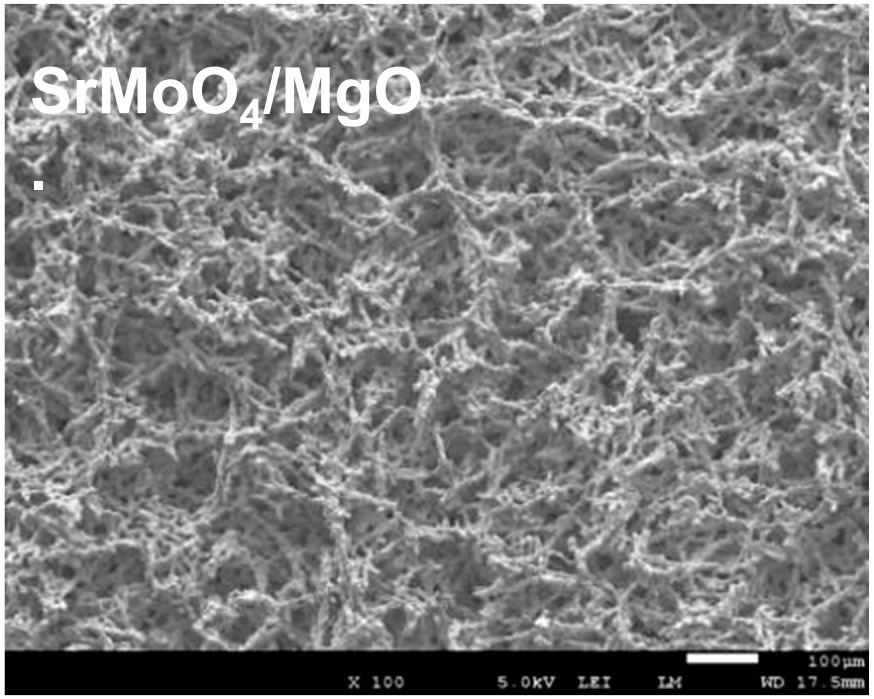

- Coarsening resistant microstructure restrained.
- Porous architecture suitable for gas penetration preserved.

SO_2 Testing of $SrMoO_4$ Sensing Materials

Nano-$SrMoO_4$

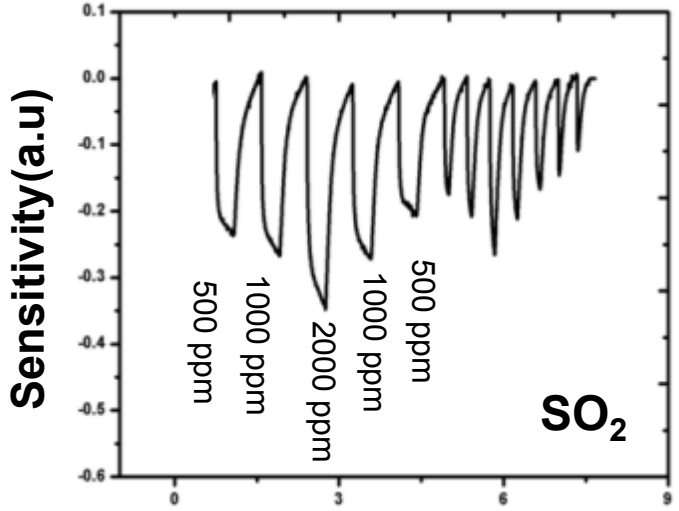

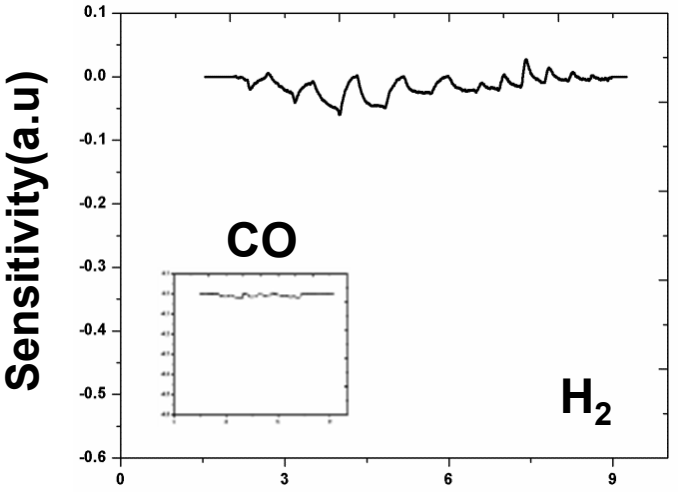

Nano-$SrMoO_4$ over MgO

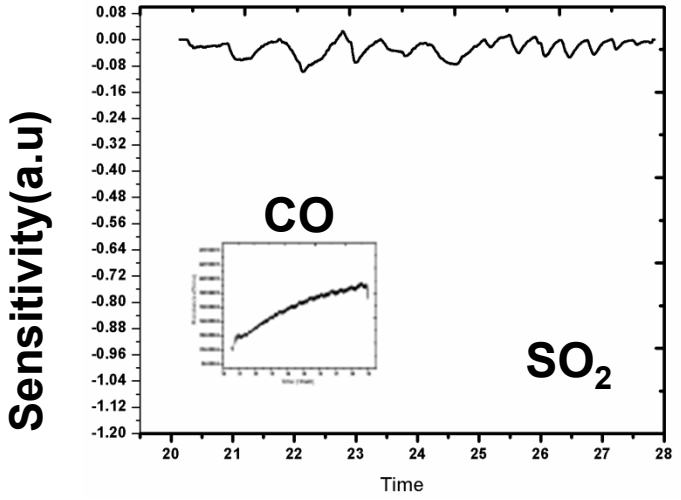

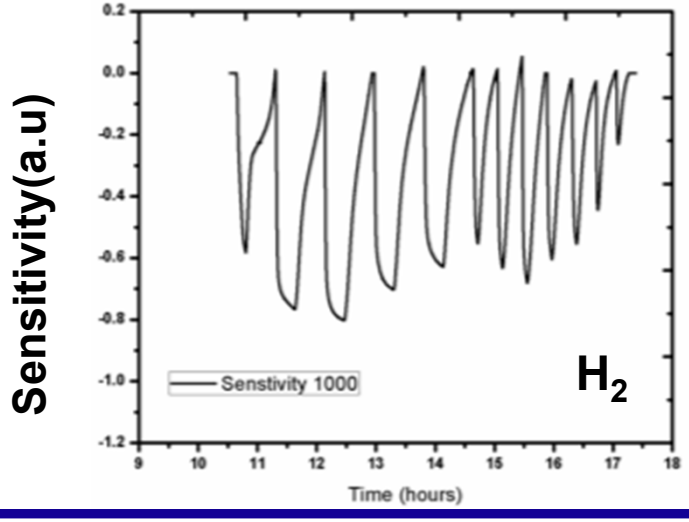

1000°C, 1%O_2

Characterization of Refractory Core Structure and Nano-$SrMoO_4$

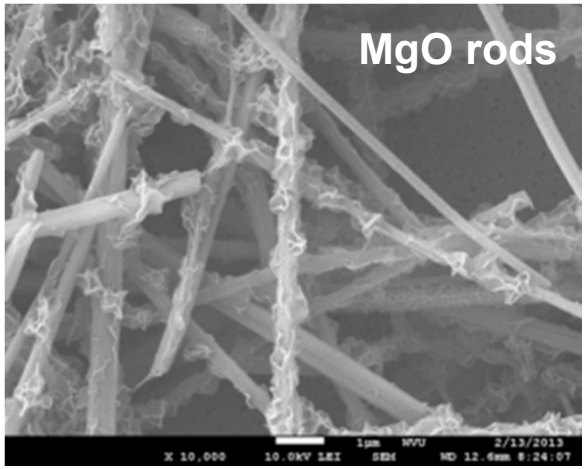

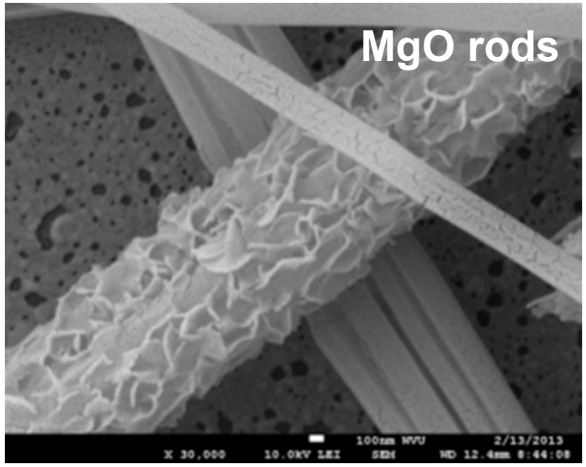

- **pH 9.5 aqueous, after 5 minutes**

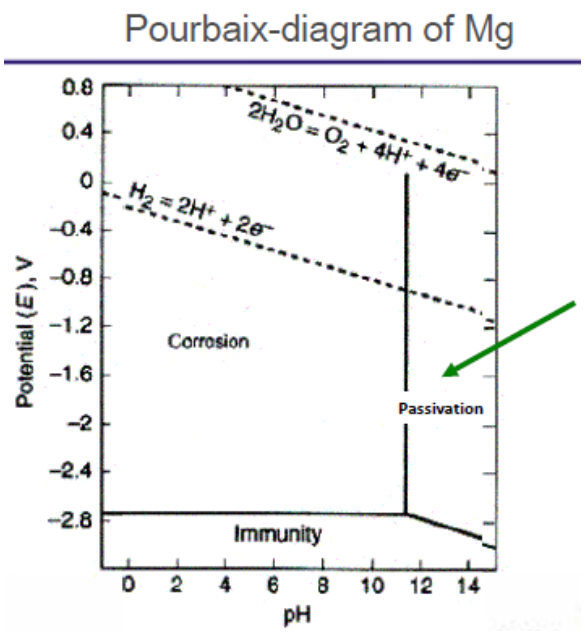

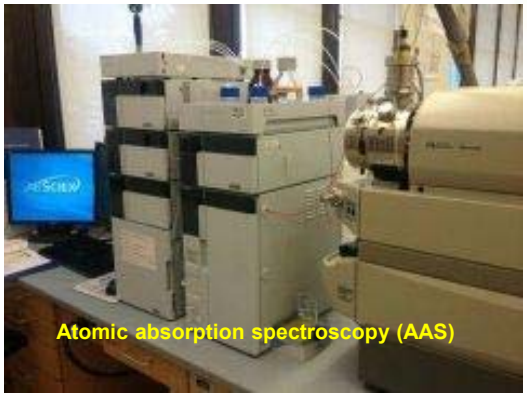

Hydrothermal Growth at pH= 9.5

- **AAS showed that ~3.1% Mg exist in $SrMoO_4$/MgO.**

- In order to have better understanding position, phase, chemical state, electronic structure of $SrMoO_4$ with Mg.

  - RAMAN
  - XPS
  - UPS
  - UV-Vis
  - TEM

Measure Work Function and Band Gap of $SrMoO_4$ and $SrMoO_4$/MgO

UPS= Ultra-Violet Photoelectron Spectroscopy: Work function

$SrMoO_4$ nano: 9.3 eV
$SrMoO_4$/MgO : 7.7 eV

Uv-Vis: Band-gap

$SrMoO_4$ nano: 3.6 eV
$SrMoO_4$/MgO : 3.2 eV

•Charge exchange between solid surface and adsorbed species depends on the **solid surfaces`s work function.**

- Chemical environment ,
- Defect structure,
- Vacancy concentration
- Cation oxidation state.

Mg incorporation to $SrMoO_4$ lattice affects electronic state.

***Physics, Chemistry and Technology of Solid State Gas Sensor Devices Andreas Mandelis, Constantinos Christofidos, 1993

XPS Depth Profile of $SrMoO_4$/(MgO)

•The data was collected through the depth of the micro-rod of $SrMoO_4$ over MgO.

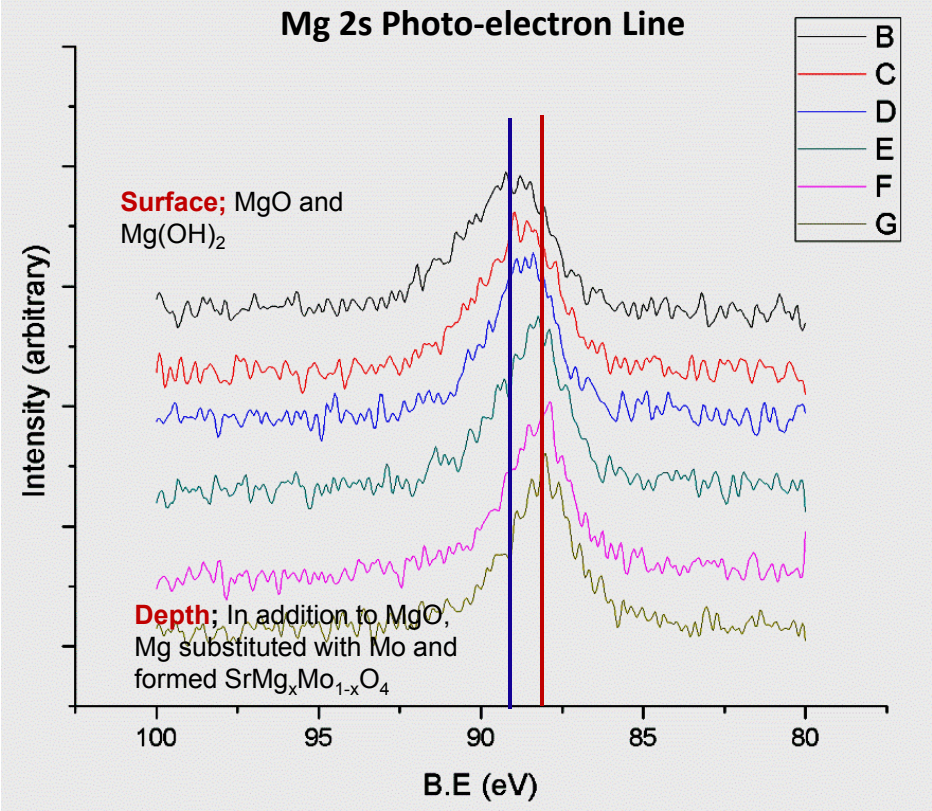

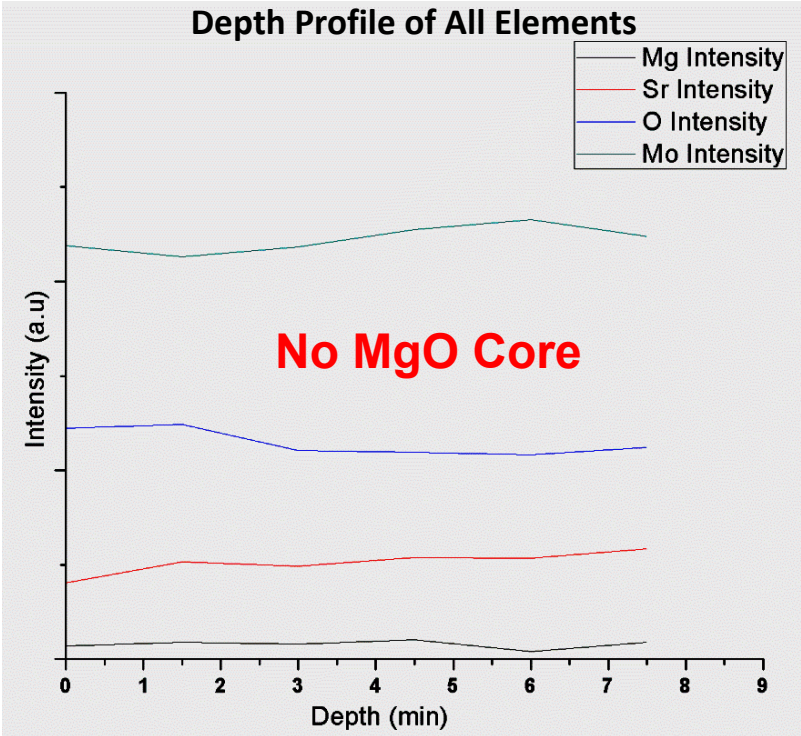

•From surface to 4.5 % to depth 4%, concentration profile of Mg via XPS.

- Mg at surface as $MgO/Mg(OH)_2$ and substituted within $SrMoO_4$.
- 17% of the O^{2-} was located on unlattice (interstitial) locations by XPS O1s. This is also further supports the lower work function value measured in the case of $SrMoO_4$/MgO.

Sulfate formation on Nano-$SrMoO_4$/(MgO)

XPS analysis of S and O positions from full scale SO_2 tested $SrMoO_4$/MgO sensor

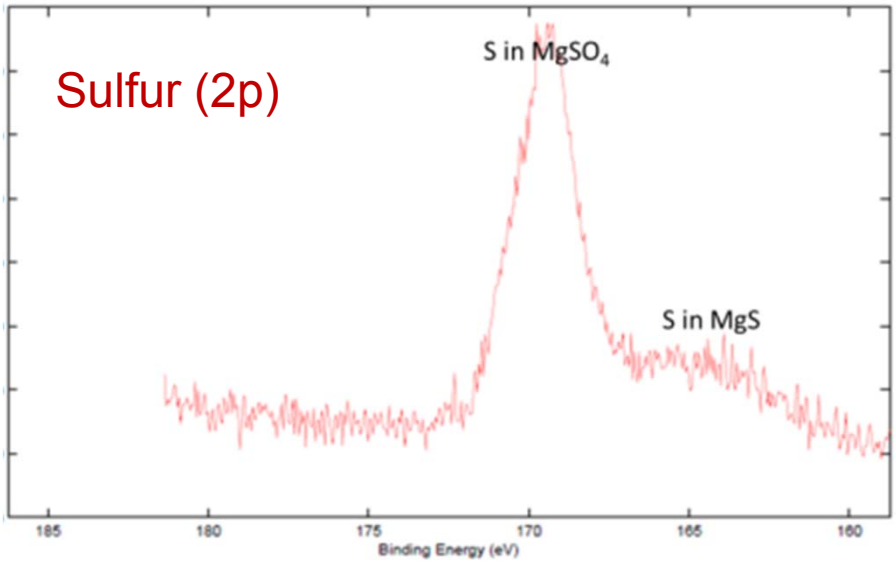

The binding energies of sulfur in $MgSO_4$ and MgS are 168.9 and 165.0 eV, respectively. The values are in an excellent match with the literature

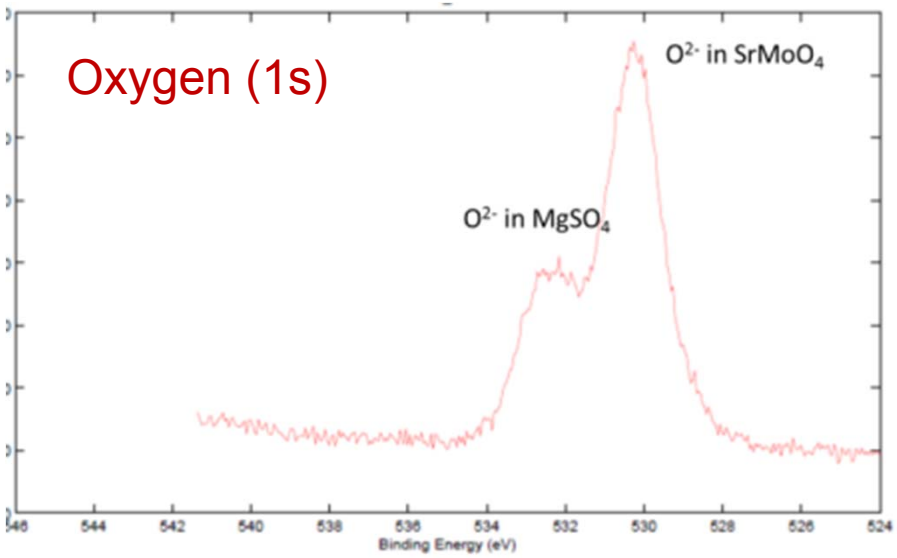

O^{2-} peak position in magnesium sulfate ($MgSO_4$) and reported that the value is 532.3 eV, which is higher than ordinary peak position of the O found in oxides.

- Metastable MgS phase fomation on the surface reacts with oxygen to form the corresponding sulfate ($MgSO_4$), and/or $MgSO_4$ can form from, MgO, SO_2 and O_2.
- $MgSO_4$ is impermeable to further SO_2 diffusion.
- $MgSO_4$ quite stable at temperatures >500 °C; stable even in regenerative cracking conditions

S. Sugiyama, T. Miyamoto, H. Hayashi and J. B. Moffat, *Bull. Chem. Soc. Jpn.* , vol. 69, p. 235, 1996.

J. F. Moulder, W. F. Stickle, P. E. Sobol and K. D. Bomben, Handbook of X-Ray Photoelectron Spectroscopy, Chigasaki, Japan: ULVAC-PHI. Inc., 1992-1995.

Mechanism of H_2 and SO_2 Selectivity?

SO_2 Selectivity of Nano-$SrMoO_4$

- Selective to sulfur: Mo highly selective to sulfur species to form metastable sulfide/sulfate.

- Low H_2 adsorption: $SrMoO_4$ shows low H_2 surface adsorption which limits electrochemical reactions *(confirmed with TPR work).*

H_2 Selectivity of Nano-$SrMoO_4$/(MgO)

- Non-selective to sulfur: MgS, metastable phase fomation on the surface; reacts with oxygen to form the corresponding sulfate ($MgSO_4$), which reduces further SO_2 adsorption and diffusion.

- High H_2 adsorption: MgO is particularly reactive to adsorption of H_2 and participates in spillover reaction to $SrMoO_4$ surface *(confirmed with TPR work).*

- Reaction with H_2: Mg incorporated into $SrMoO_4$ increased H_2 interaction with unlattice (interstitial) oxygen to alter n-type response.

*E. T. Türkdoğan, B. B. Rice, Sulfide and Sulfate Solid Solubility in Lime, Magnesia and Calcined Dolomite: Part II. Free Energy of Formation of Magnesium Sulfate, Metallugic Transactions, 1974.
**Hydrogen storage properties of Mg-based composites prepared by reaction ball milling, M Kandavel and S Ramaprabhu1, J. Phys.: Condens. Matter, 2006.
*** Dekker Encyclopedia of Nanoscience and Nanotechnology, Volume 3, pp.1913, james A. Schwarz, Cristian I. Contescu, Karol Putyera.

Micro-Sensor and -Array Fabrication and Testing

Micro-sensor Array Fabrication

1) Negative lithography used for micro-molds
   - SU8-25 (Microchem)
     - From 20-90 µm depth depending on spin rate
   - OAI UV Flood Exposure System
   - SU8 developer
2) Sensing material is casted into mold.
3) Mold is burned off and material is sintered or bonded to substrate.

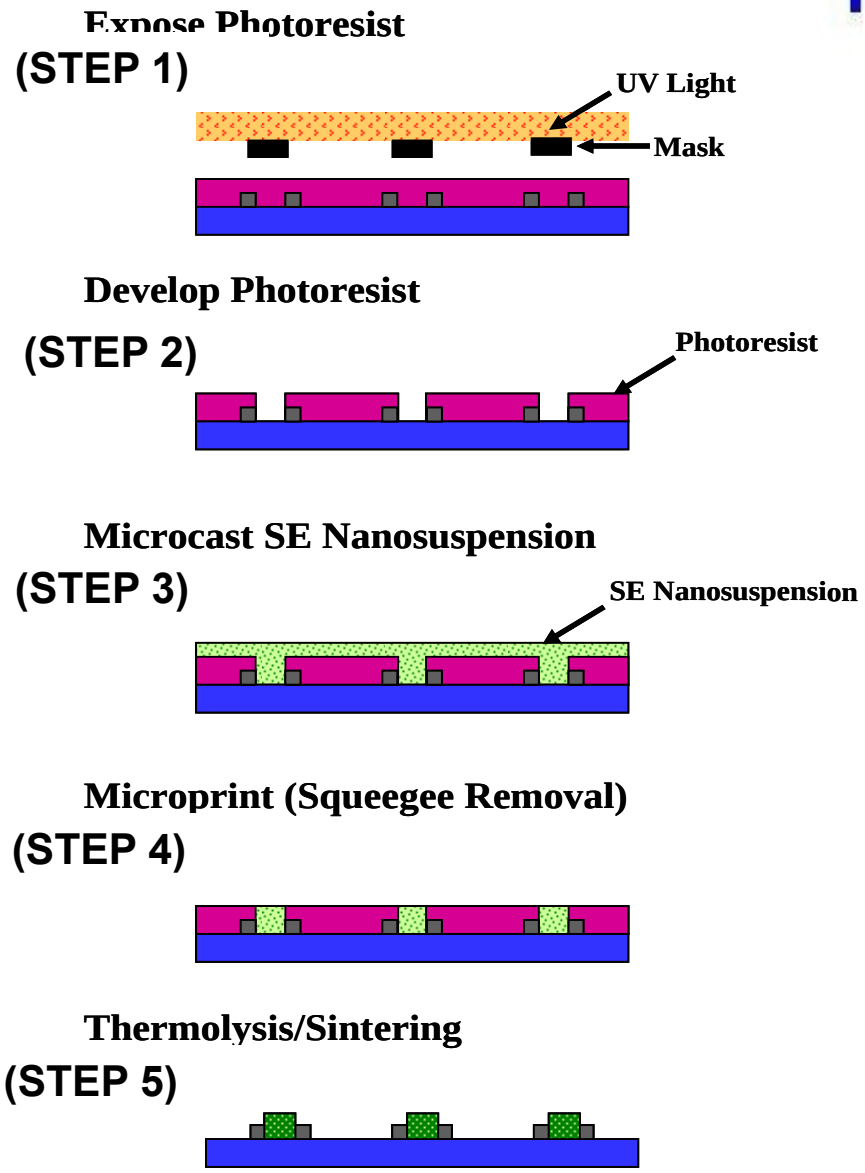

Micro-Casting - SEM

•Casted single layer on YSZ substrate

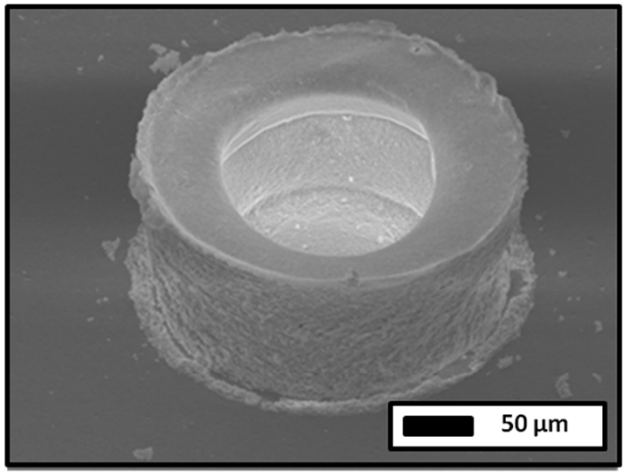

(a)

•Casted double layer on YSZ substrate

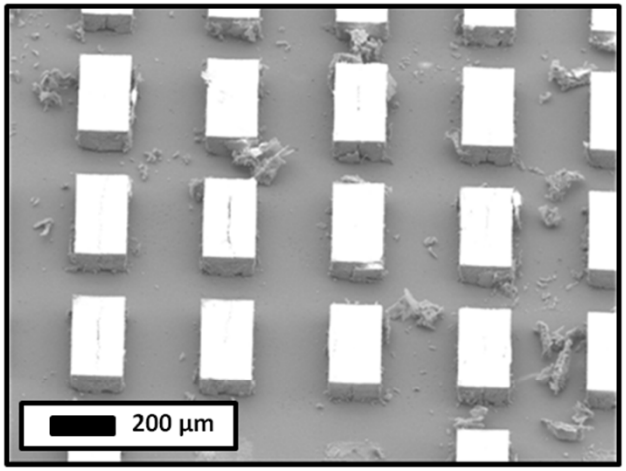

(b)

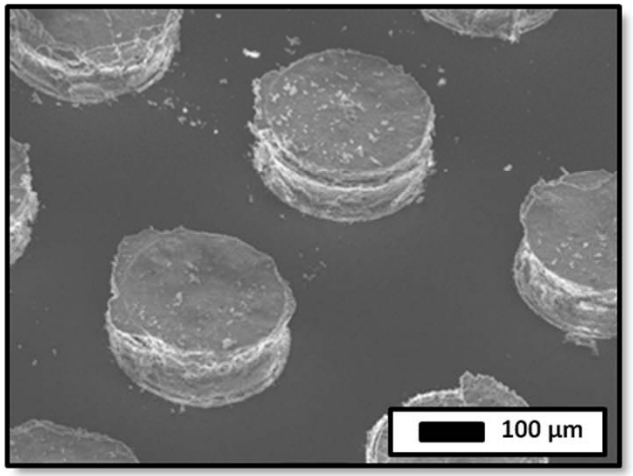

(c)

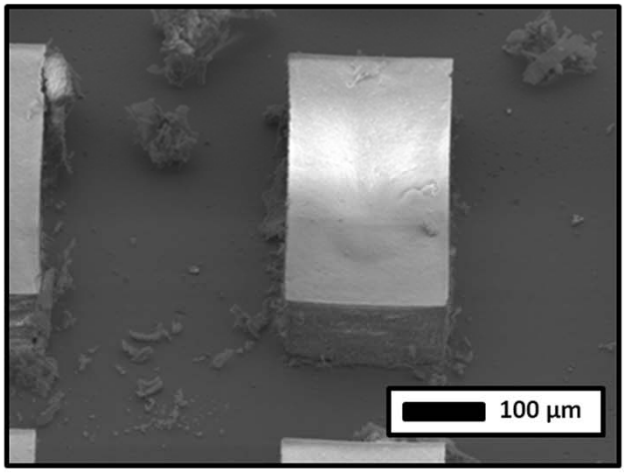

(d)

Micro-casting of Sensor Arrays

Nano-SnO_2

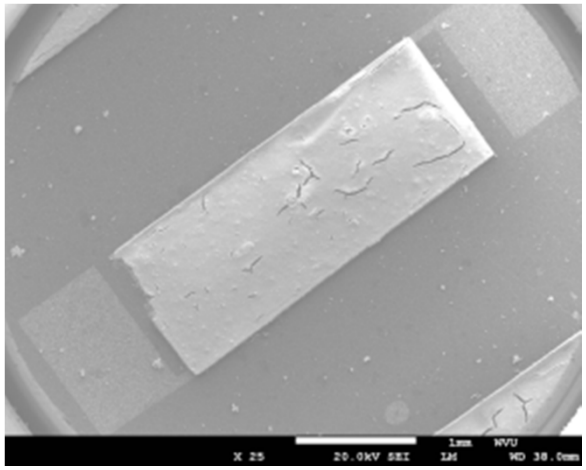

Nano-10% SnO_2/90% $Gd_{1.8}Y_{0.2}Zr_2O_7$

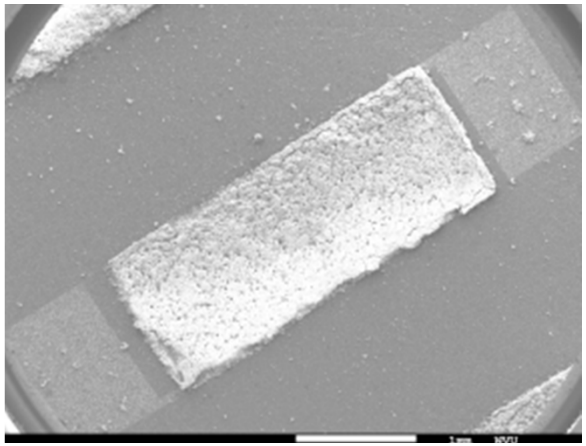

Nano-$Gd_2Zr_2O_7$

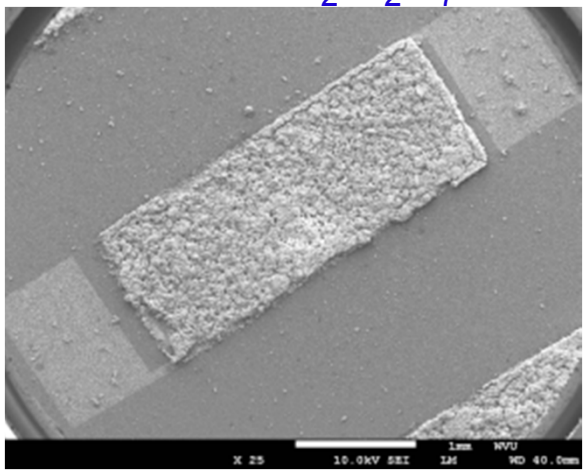

Nano-SnO_2 and $Gd_{1.8}Y_{0.2}Zr_2O_7$ Arrays

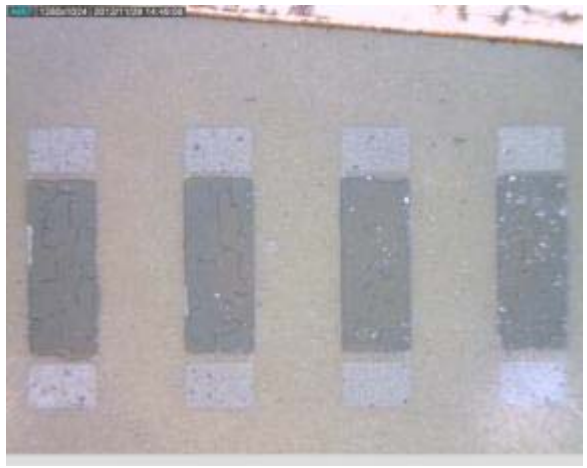

Micro-sensor and arrays fabricated with nano-SnO_2 and nano-SnO_2/zirconate materials.

Micro-sensors array for H_2, H_2S and SO_2

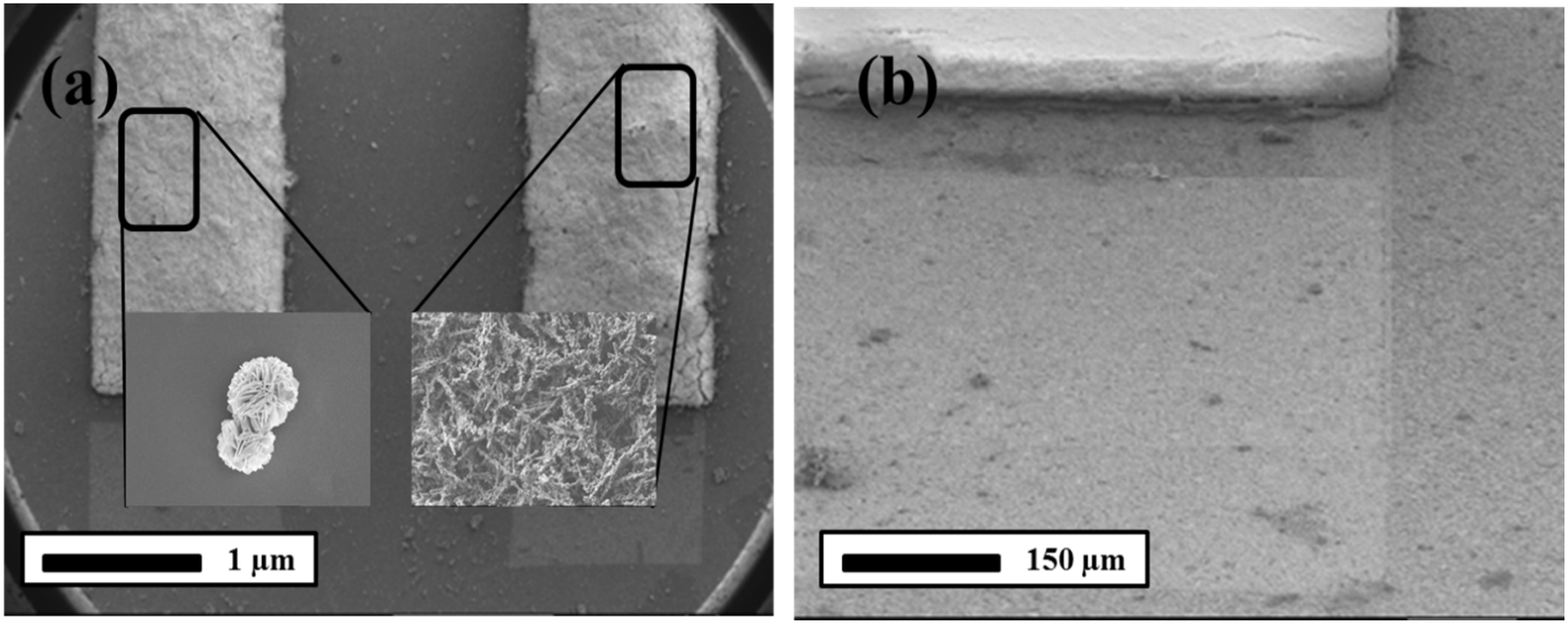

$SrMoO_4$/MgO and $SrMoO_4$ nanoflowers sensing material deposited over Zr/Zr+Pt/Pt type microelectrode and close-up of edge.

Testing of Microsensor for H_2

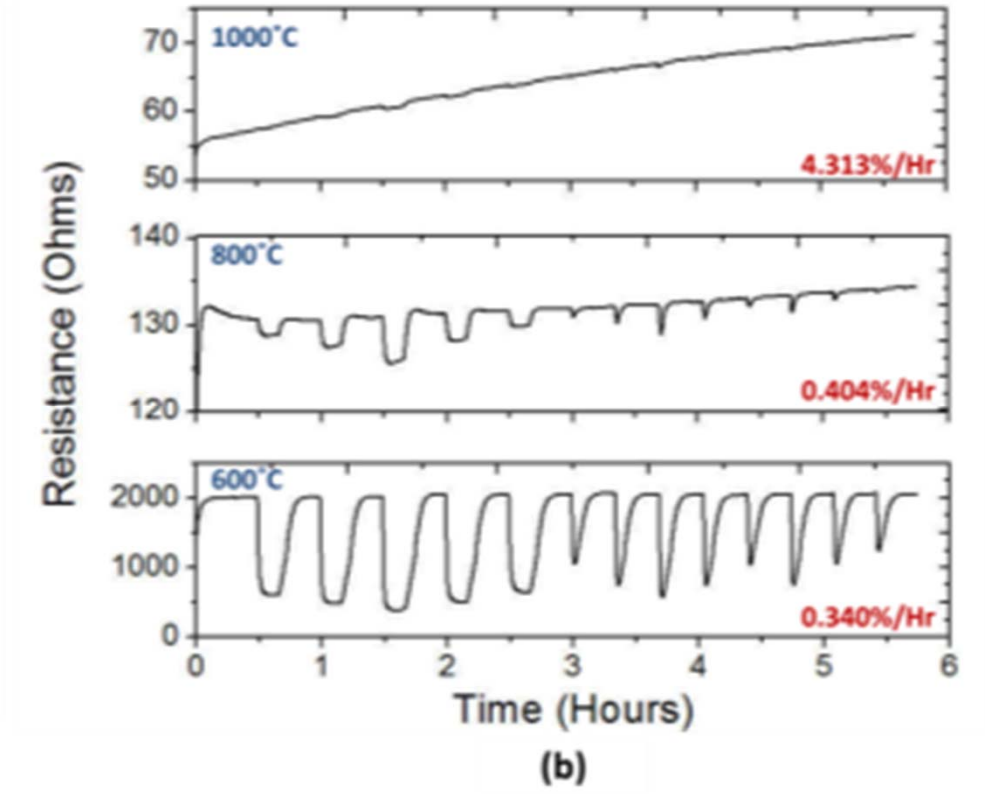

- Micro-IDEs were fabricated by sputtering process.
- 29 fingers were spaced 50 µm apart with a sensing area of 1.2 mm x 3 mm.

SnO_2 sensor

- Sensitivity of 0.812 and 0.010 at 600 and 800°C to 4000 ppm of H_2

Compared to Macro-Sensors

~63% increase in response rate

~200% increase in sensitivity

N_2 with ppm H_2 (10% oxygen atmosphere)

Testing of Microsensor for H_2, H_2S and SO_2

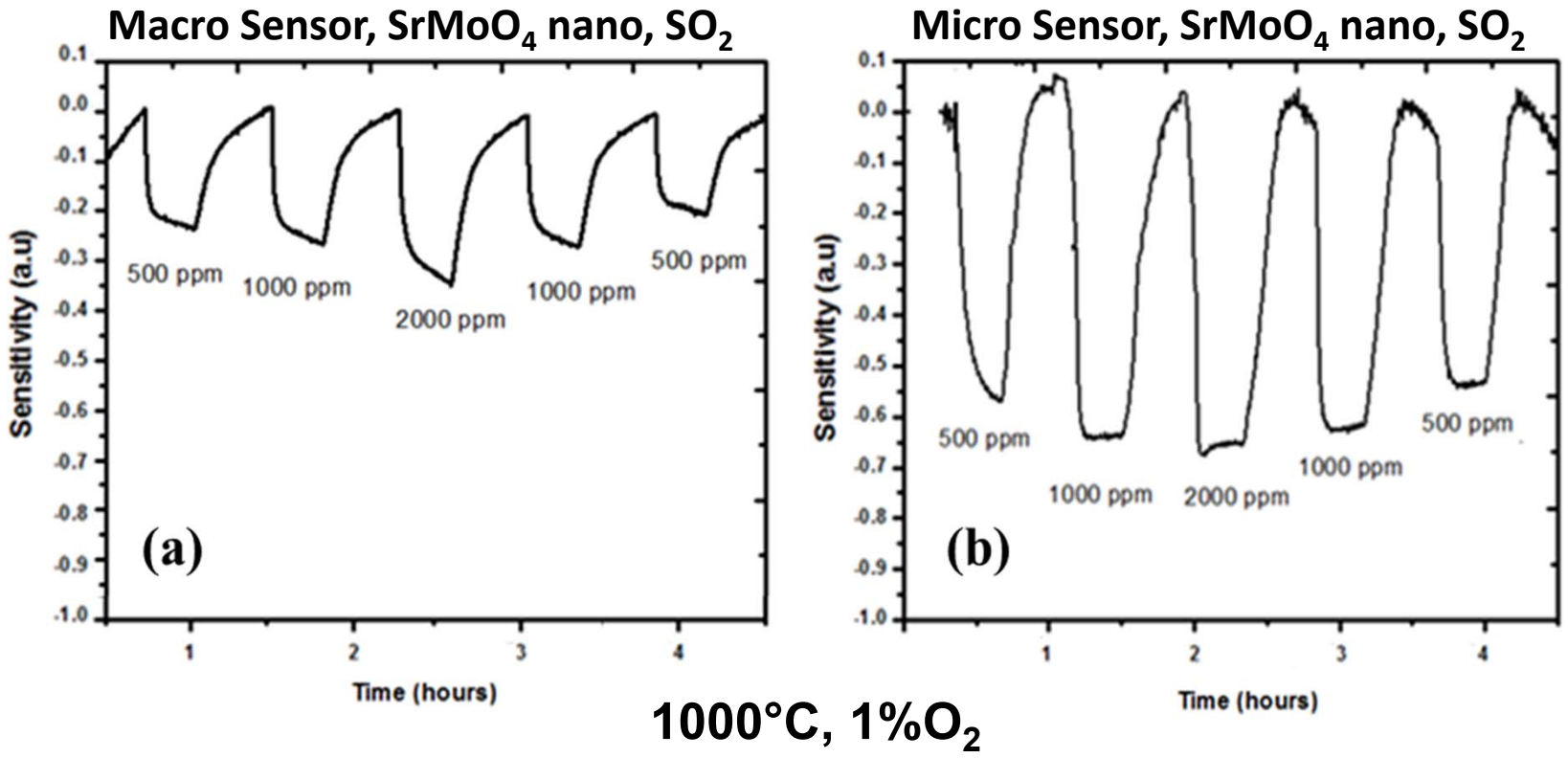

1000°C, 1%O_2

Usage of micro platform of $SrMoO_4$ nanoflowers, the increase in sensitivity was up to 65%.

Testing of Microsensor for H_2, H_2S and SO_2

Macro Sensor, $SrMoO_4/MgO$, H_2

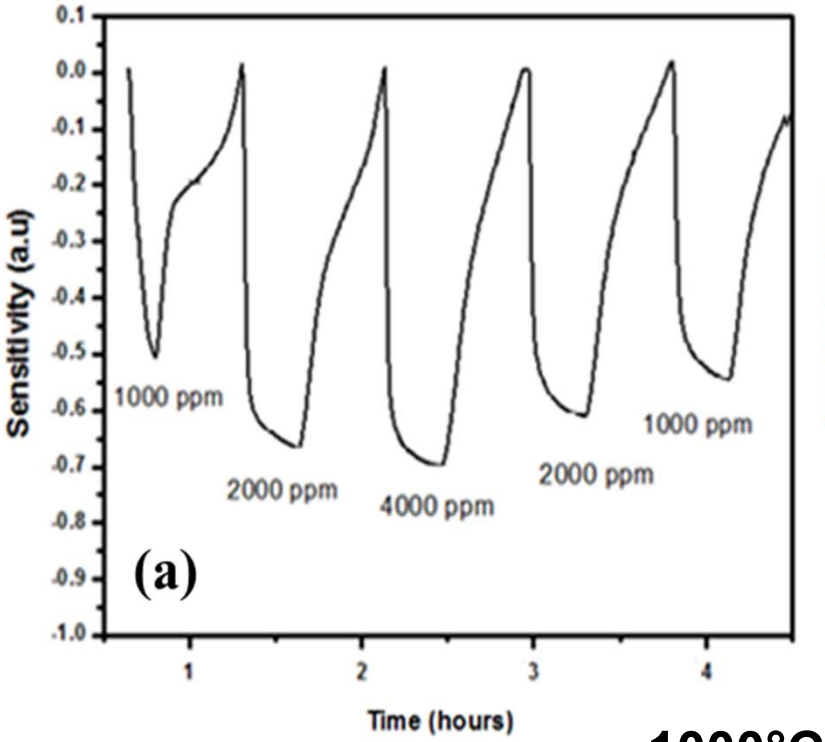

Micro Sensor, $SrMoO_4/MgO$, H_2

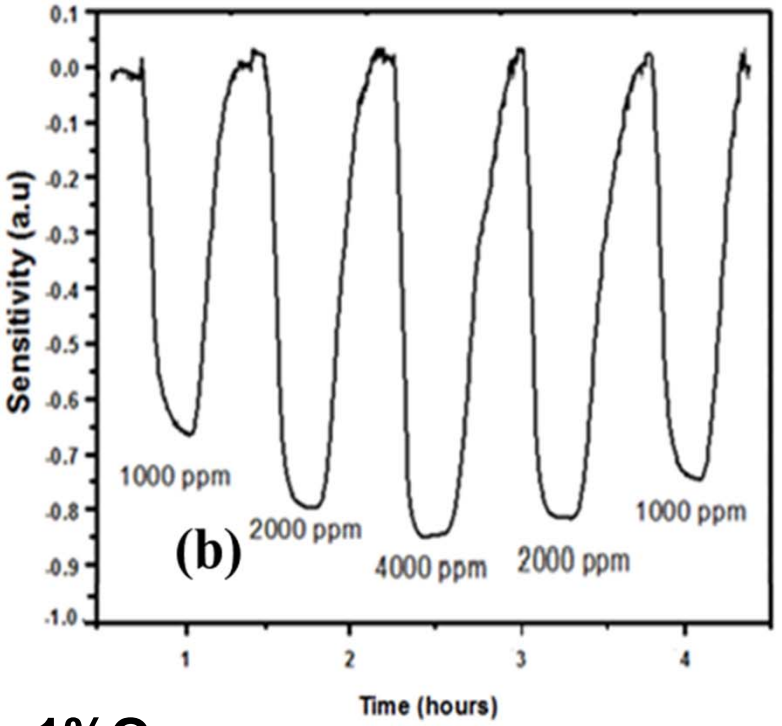

1000°C, 1%O_2

$SrMoO_4/MgO$ reported a sensitivity increase of 40%.

Work Summary

1. High-temperature interdigitzed electrodes (IDEs).

- *High temperature micro-IDEs (stable to 1200℃) were developed and method for micro-patterning.*

2. Sensing Materials for Sulphur Compounds.

- Ternary tungstates and molybdates were synthesized at the micron- and nano-scale, and tested for SO_2 and H_2S.
- High sensitivities were measured >800°C, but the as-synthesized nanomaterial morphologies were not stable.

3. High-temperature Stabilization of Ternary Mo/W Nanomaterials

- Nano-$SrMoO_3$ (which showed high sensitivity to SO_2) was grown over nano-fiber MgO to form stable nano-morphology.
- Selective sensing to H_2 (with high sensitivity, >80% for high ppm).

4. Micro-sensors and Array Fabrication

- Micro-molding process was developed to deposit forms down to ~10μm.
- Micro-sensors and basic arrays (with synthesized nanomaterials) were fabricated on stable micro-IDEs.
- 50-200% increase in sensitivity and >50% increase in response rate.

Acknowledgments

- This research was funded by US Department of Energy University Coal Research (UCR) program under contract DE-FE0003872. We want to thank DOE for their support.

- WVU Shared Research Facilities.

- We also would like the acknowledge Dr. Kolin Brown, Dr. Wei Ding, Mr. Harley Hart for their assistance.

Coating Type	As Deposited	1 h	5 h	15 h	24 h	48 h
Ti+Pt	210	561	--	--	--	--
Ta+Pt	192	442	3106	--	--	--
Zr+Pt	201	234	684	--	--	--
Hf+Pt	207	244	--	--	--	--
L-Zr+Pt	252	-	-	315	391	--
Hf/L-Zr+Pt	247	-	-	-	211	624
Zr/Zr+Pt/Pt	219	257	289	508	--	--

Work Function and Band Gap of $SrMoO_4$ and $SrMoO_4$/MgO

• **Electronic aspect aspect of the Mg incorporation to $SrMoO_4$ lattice,** Important consequences of Mg incorporation can be observed in electronic aspects; therefore, the work function and band-gap measurements were conducted via ultraviolet photoelectron spectroscopy (UPS) and ultraviolet-visible light absorption spectrum (Uv-Vis), respectively

UPS: Work function ($q\phi_m$)

•Barrier height is that the gap between conduction and fermi levels, $q\phi_b = q(\phi_m - \chi)$

$SrMoO_4$ Micron : 8.2 eV
$SrMoO_4$ Nano: 9.3 eV
$SrMoO_4$ + MgO : 7.7 eV

•TMOs surface engages charge exchange (e^-) with absorbed material.

•Charge exchange between solid surface and absorbed species depends on the **solid surfaces`s work function.**

- Chemical environment , defect structure, vacancy concentration and cation oxidation state.

- Quantum confinement results in an increase in the band gap, which may explain in the increase in the band gap nano-$SrMoO_4$-nano compare to micro-$SrMoO_4$
- Missing O from the $SrMoO_4$ during the deposition process and/or reduction in the un-lattice (interstitial) oxygen sites can cause the reduction in band-gap value. The substitution of Mg into Mo would result in opposite effect regarding to the band-gap height
- In order to explain reduction in the band gap value from $SrMoO_{4-\delta_1}$ nano to $SrMoO_{4-\delta_2}$+MgO work functions were determined Average cation oxidation state proportional to work function (ϕ_m). In other words, oxygen deficiency is disproportional to work function (ϕ_m).

Uv-Vis:Band-gap

$SrMoO_4$ Micron
Band-gap: 3.9 eV
Un-lattice could not be measured due to secondary SrO phase

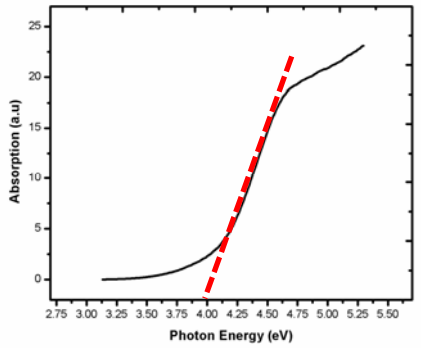

$SrMoO_{4-\delta 1}$ nano
Band-gap: 3.6 eV
20% O^{2-} located at un-lattice locations, un-Lattice oxygens can be thought as adsorbed O^{2-} down to 10 nm from surface

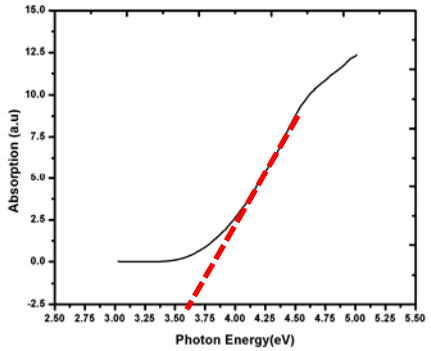

$SrMoO_{4-\delta 2}$+MgO
Band-gap: 3.2 eV
17% O^{2-} located at un-lattice locations
$\delta 2 > \delta 1$

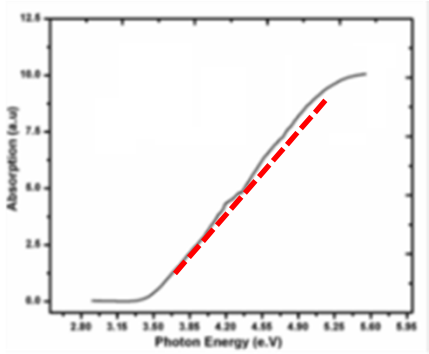

- Physics, Chemistry and Technology of Solid State Gas Sensor Devices Andreas Mandelis, Constantinos Christofidos, 1993
- Szczancoski et al., Chemical Engineering Journal, 140, 2008.
- Yan et al., Journal Physical Chemistry, 113, 2009
- Mark T. Greiner, et al., Advanced Functional Materials, 22, 20120

Typical Electrochemical Sensing Mechanisms

•**Possible Reactions occur during sensor operation**

H_2S

$$H_2S_{(ads)} + 3O^{2-}_{(s)} \rightarrow SO_{2(g)} + H_2 + 3e^-$$

$$H_2S_{(ads)} + 3O^{2-}_{(s)} \rightarrow SO_{2(g)} + H_2 + 6e^-$$

$$H_2S_{(ads)} + O^-_{(ads)} \rightarrow H_2O + SO + e^-$$

$$H_2 + O^-_{(ads)} \rightarrow H_2O + e^-$$

$$V_O^X \rightarrow V_O'' + 2e^-$$

SO_2

$$SO_2 + O_{(ads)} \rightarrow SO_3 + V_O^X$$

$$SO_2 + O_{(lattice)} \rightarrow SO_3 + V_O^X$$

$$V_O^X \rightarrow V_O'' + 2e^-$$

$$SO_{2(gas)} + O_{2(gas)} \rightarrow SO_{3(gas)}$$

$$SO_3 + e^- \leftrightarrow SO^-_{3(ads)}$$

H_2

$$H_{2(g)} + O^X_{O\,(bulk)} \leftrightarrow H_2O_{(g)} + V_O^{\cdot\cdot} + 2e^-$$

$$H_{2(g)} + O^{2-}_{(ad)} \leftrightarrow H_2O_{(g)} + 2e^-$$

$$H_{2(g)} + O^-_{(ad)} \leftrightarrow H_2O_{(g)} + e^-$$

$$^1/_2 H_{2(g)} + OH^-_{(ad)} \leftrightarrow H_2O_{(g)} + e^-$$

$$^1/_2 O_{2\,(g)} + V_O^{\cdot\cdot} + 2e^- \leftrightarrow O^X_{O\,(Bulk)}$$

$$^1/_2 O_{2\,(g)} + e^- \leftrightarrow O^-_{(ad)} \qquad (or\ OH^-_{(ad)})$$

$$H_{2(g)} \leftrightarrow 2H^+_{(ad)} + 2e^-$$

$$^1/_2 O_{2\,(g)} + H_{2(g)} \leftrightarrow H_2O_{(g)}$$

*S. K. Pandey *et. al.*, Trends in Analytical Chemistry, Vol. 32, 2012

RAMAN Characterization of $SrMoO_4$

- RAMAN technique is sensitive to vibrational modes in crystal structure, substitutional solid solution formation such as, $SrMg_xMo_{1-x}O_4$ and/or doping level of Mg incorporation to $SrMoO_4$ lattice.

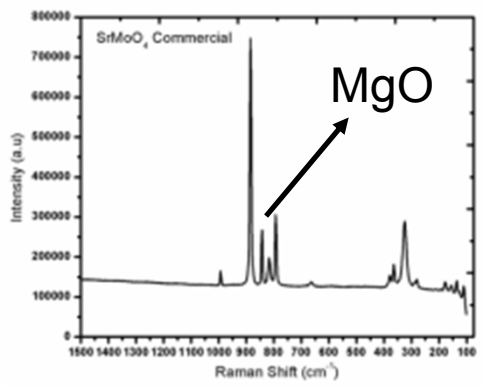

$SrMoO_4$ commercial RAMAN Spectrum

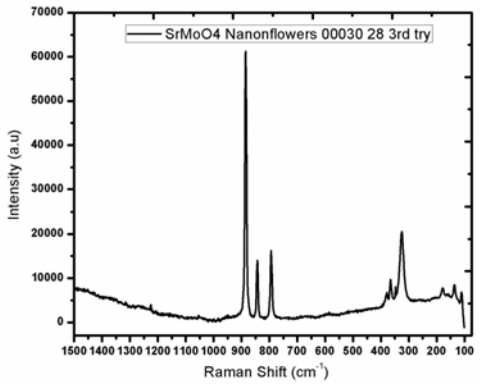

$SrMoO_4$ nano

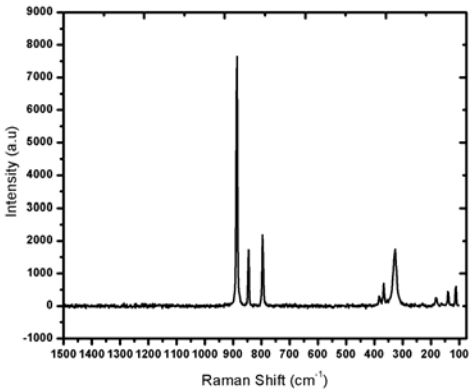

$SrMoO_4$/MgO

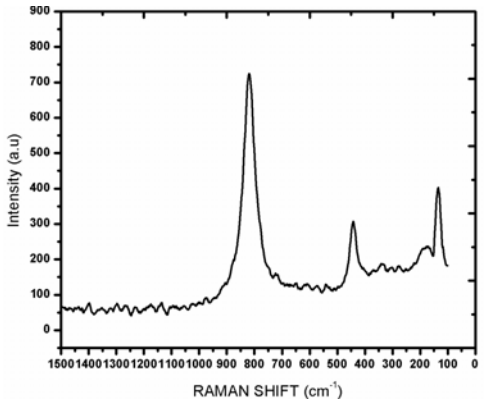

SMM RAMAN Spectrum

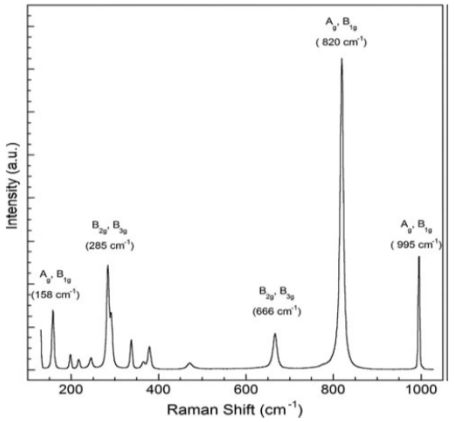

MoO_3 RAMAN Spectrum

Table 4 Raman vibrations of $SrMoO_4$ and $SrWO_4$ and their prominence (*)

Raman vibration	Wavenumber (cm^{-1})	
	$SrMoO_4$	$SrWO_4$
$\nu_1(A_g)$	888.04*	921.72*
$\nu_3(B_g)$	846.29	838.40
$\nu_3(E_g)$	796.92	794.37
$\nu_4(B_g)$	368.60	371.82
$\nu_2(A_g)$	327.23	337.60
$\nu_{Ex}(A_g)$	180.40	189.66

- Raman is capable of detecting down to 0.5% substitution in $SrMoO_4$ lattice as main peaks get broad
- MgO secondary phase formation possible.

Nano-$SrMoO_4$/MgO, Raman Spectrum

Surface Interaction Kinetics

D_{chem} and K_{chem} values for 500, 1000 and 2000 ppm of SO_2-$SrMoO_4$ nano.

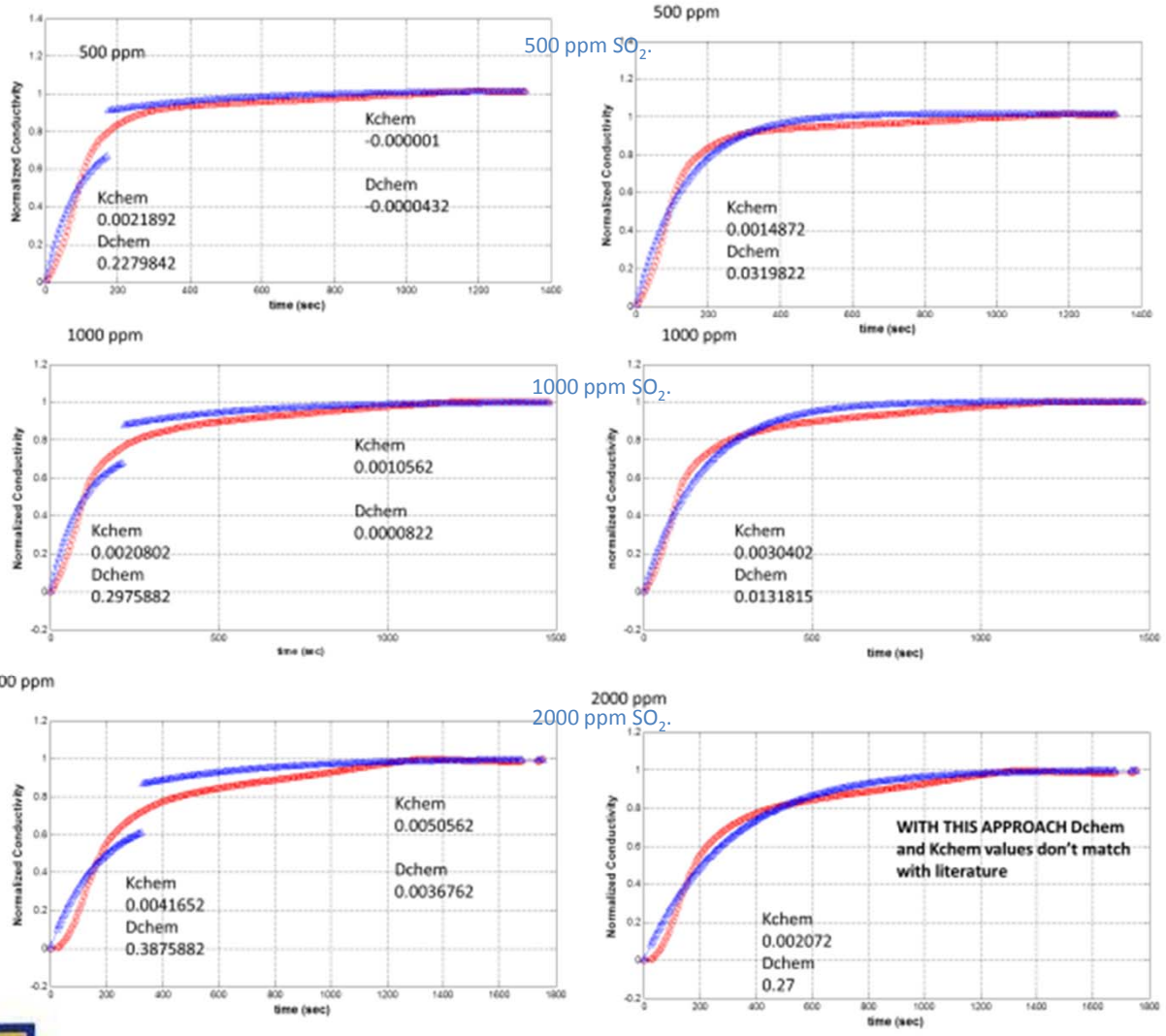

Surface interaction is diffusion-like process, amount of interstitials are determined by XPS, and it is like etching process, Sudden increase in the conductivity is related to pure surface interaction of the approaching SO_2 molecules and interstitial and/or chemically physically adsorbed oxygen. Adsorption of SO_2 is very limited at 1000°C, desorption of it has maximum at 500°C. Second part is diffusion related. The second side of the given graphs, the conductivity increase is related to diffusion of the SO_2 and its interaction with the lattice oxygen.

Micro-sensor Array Fabrication

SU8 Micro-mold

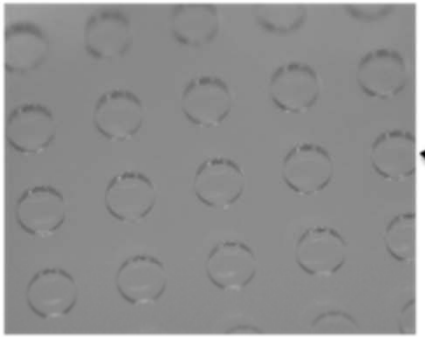

Expose Photoresist

(STEP 1)

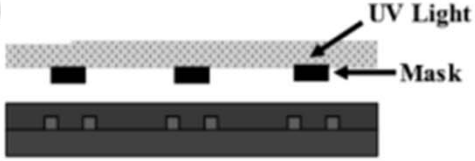

Develop Photoresist

(STEP 2)

Microcast SE Nanosuspension

(STEP 3)

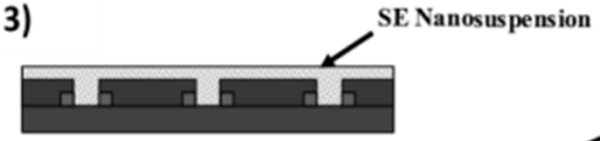

Microprint (Squeegee Removal)

(STEP 4)

Thermolysis/Sintering

(STEP 5)

Micro-casted into Micro-molds

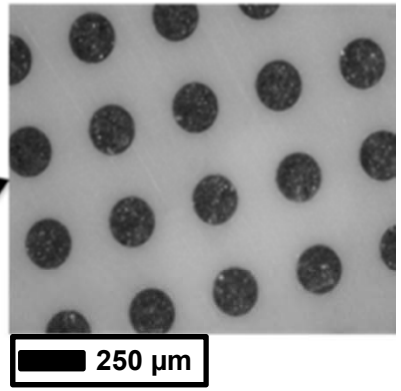

Thermally Processed Features

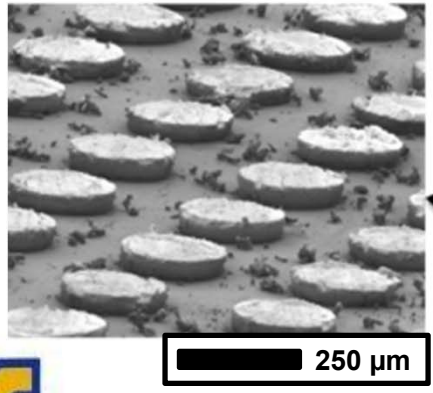

Micro-Casting - SEM

•Casted single layer on YSZ substrate

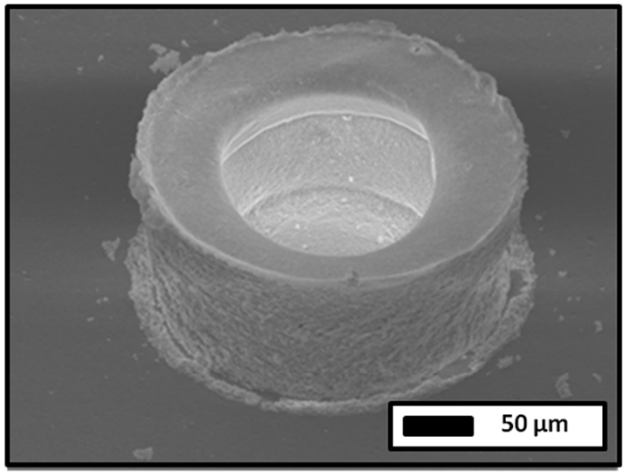

(a)

•Casted double layer on YSZ substrate

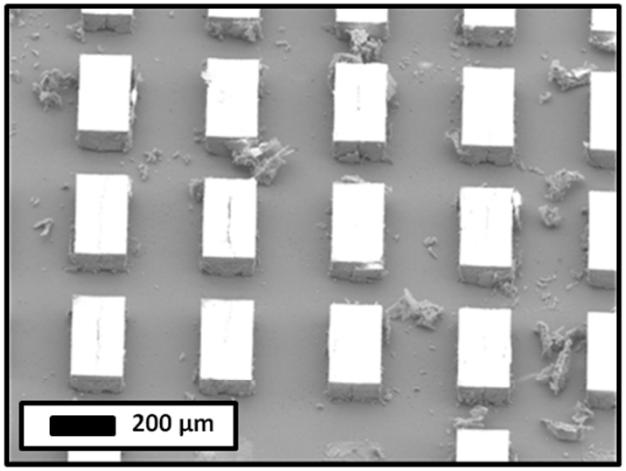

(b)

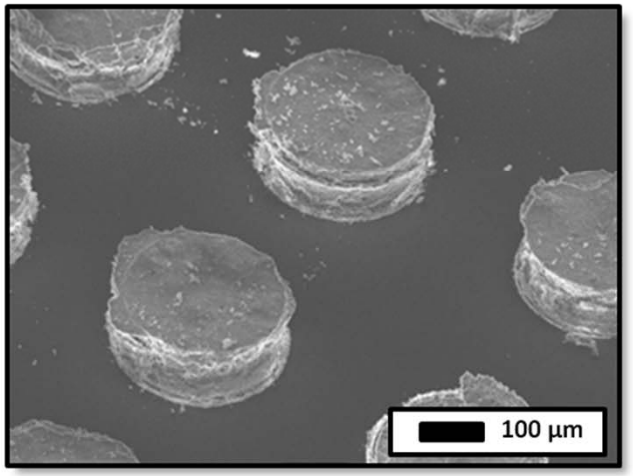

(c)

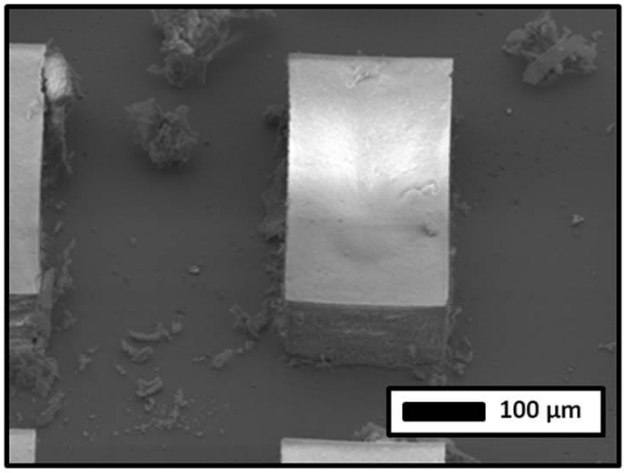

(d)

Nano-$SrMoO_4$ and MgO Composite

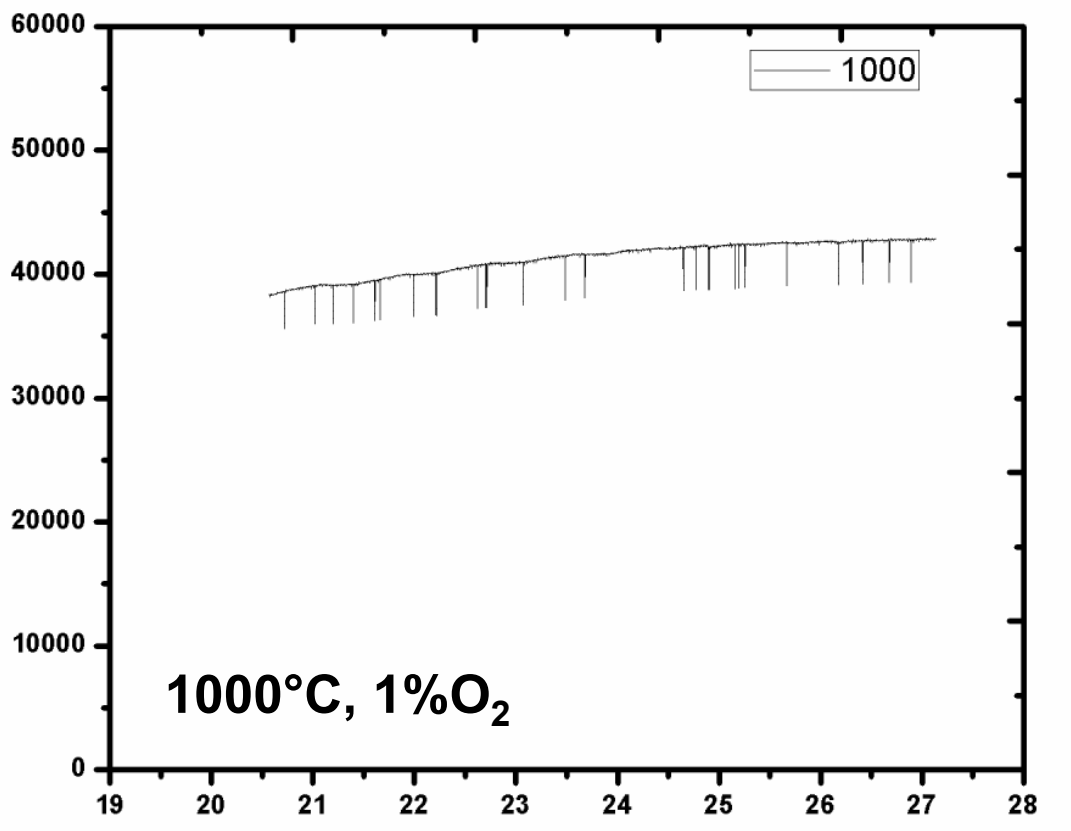

- Mixed nano-$SrMoO_4$ and nano-MgO to form particulate composite
- Not formed by hydrothermal process.

No response to pulsed 2000 ppm SO_2 in N_2!

Compositional Testing
Morphology of sintered powders

Fired to 1200°C for 2 h

- In pure GZO, particles are uniform and around <80 nm
- **10% nano-SnO_2** – 60 nm with well distributed pore network
- **50% nano-SnO_2** – 50 nm or less with increased porosity
- **90% nano-SnO_2** - particles increased to 100-300 nm
- Each system's particles size much less than pure nano-SnO_2 ~ 1 µm

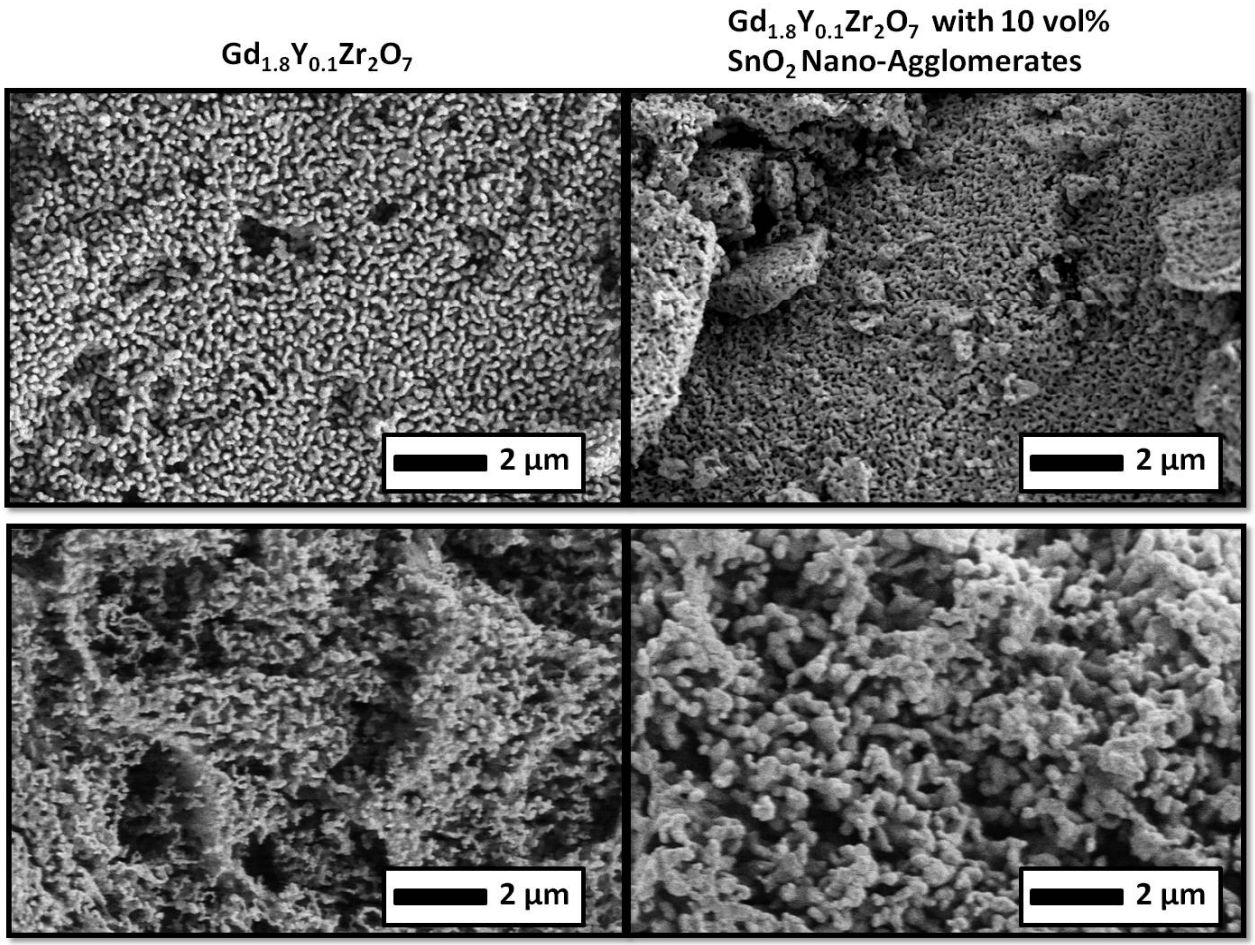

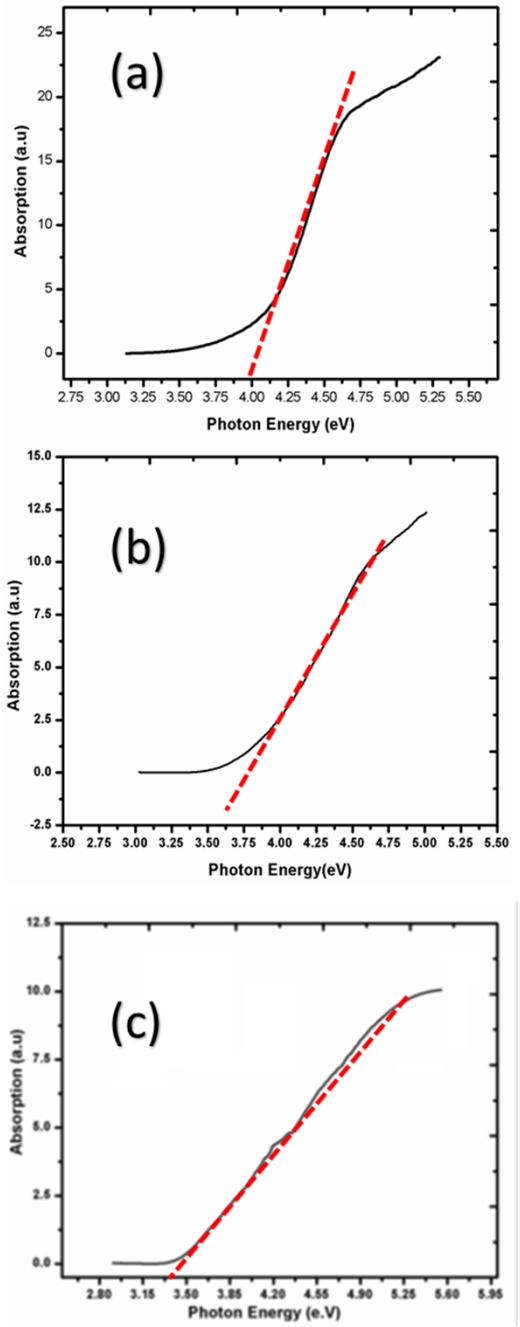

Figure 100: Band-gap measurements of (a) $SrMoO_4$-micron (b) $SrMoO_4$-nano (c) $SrMoO_4$/MgO

H_2S Sensing of Nano-$SrWO_4$ Sensing Materials

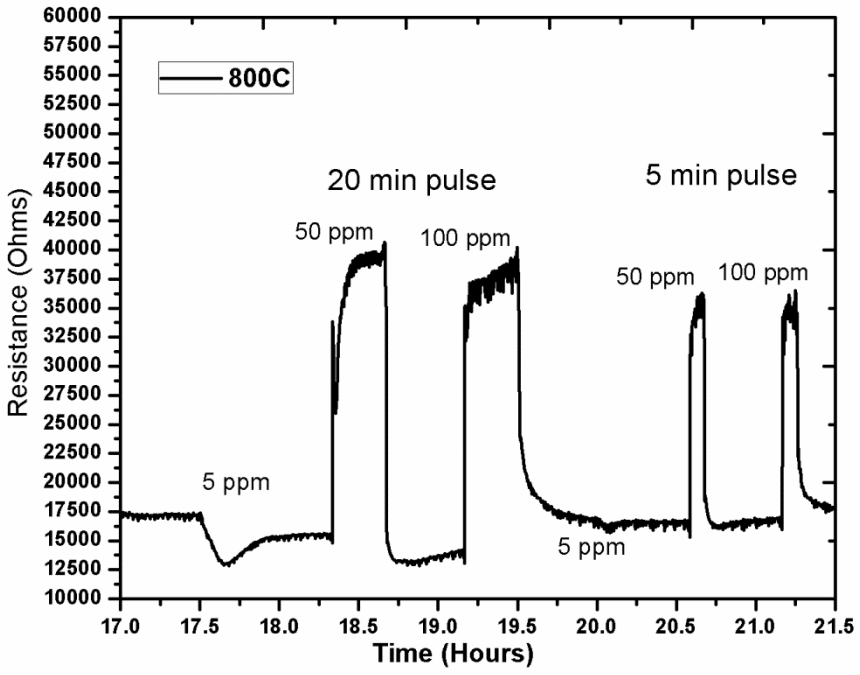

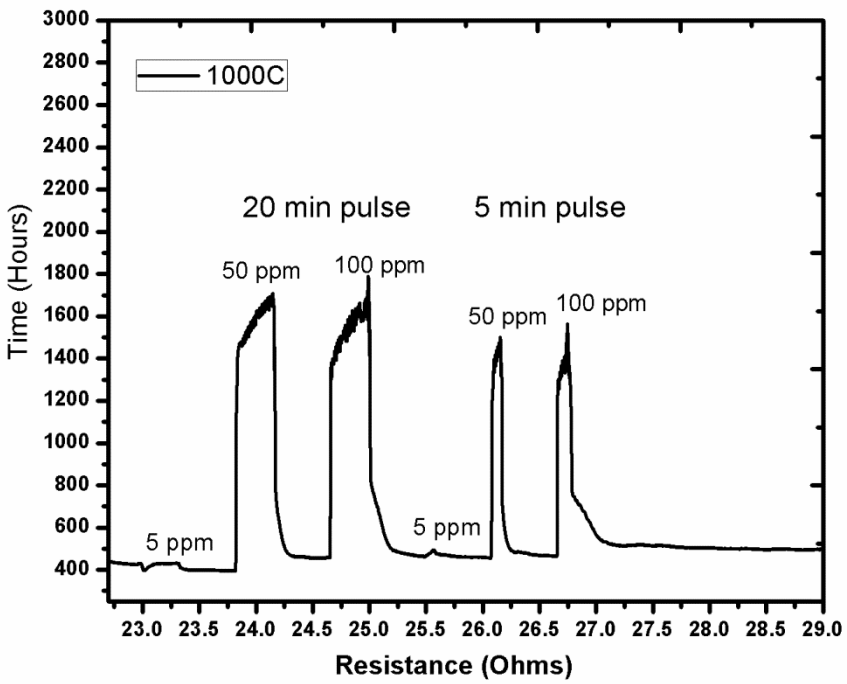

- **Sensitive towards 5, 50, and 100 ppm H_2S at 800 and 1000°C**
- **P-type behavior**
- **Long term stability (48 h testing)**

$SrWO_4$

Intermetallic formation

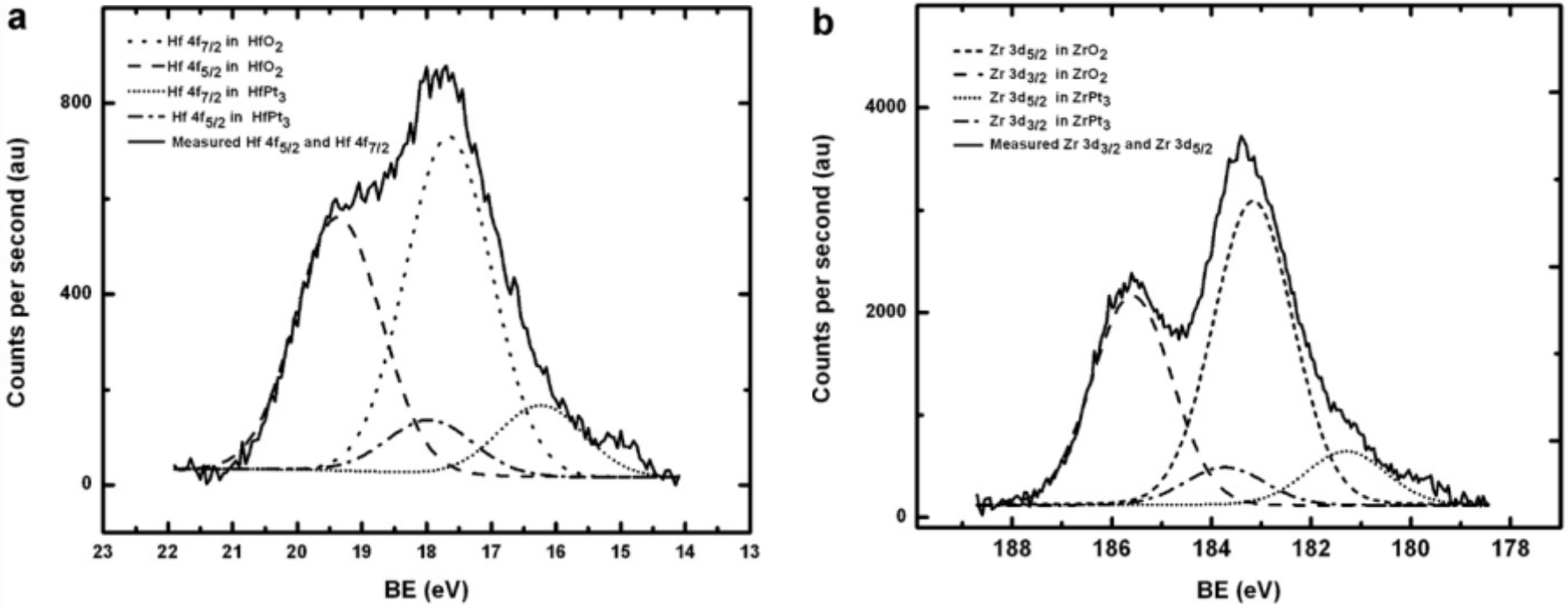

Detailed XPS scan for the (a) Hf 4f peak positions in the Hf/L-Zr + Pt sample. (b) Zr 3d peak positions in the L-Zr + Pt sample, both annealed at 1200 ◦C for 48 h.